Supplement of Atmos. Chem. Phys., 25, 17553–17580, 2025
https://doi.org/10.5194/acp-25-17553-2025-supplement

Atmospheric Chemistry and Physics
Open Access
EGU

Supplement of

Evaluation of and updates to the oxidized reactive nitrogen gaseous dry-deposition parameterization from the GEOS-Chem model, including a pathway for ground surface NO_2 hydrolysis

Brian L. Boys et al.

Correspondence to: Brian L. Boys (bboys@dal.ca)

Supplementary Material

Contents

S1 Gaseous dry deposition parameterization from the GEOS-Chem model

The dry deposition flux of gases in GEOS-Chem proceeds in grid cells in contact with the ground following an inferential technique (Eq. (1)), with species-specific deposition velocities $V_d(x)$ computed following the standard resistance-in-series approach (Eq. (2)).

Aerodynamic resistance is formulated to represent the resistance to turbulent transport of scalars within the surface layer from a reference height z (i.e., a measurement height or model grid box center) down to the roughness length z_o of the surface—the height above the zero plane displacement d where the logarithmic wind profile is assumed to extrapolate to zero (Garratt, 1992; Kaimal and Finnigan, 1994; Toyota et al., 2016; Wesely and Hicks, 1977):

$$R_a(z) = \frac{1}{ku_*}\left[\ln\left(\frac{z-d}{z_o}\right) - \Psi_h\left(\frac{z-d}{L}\right) + \Psi_h\left(\frac{z_o}{L}\right)\right], \quad \text{(S1)}$$

where k is the von Karman constant (0.4 in GEOS-Chem), u_* the friction velocity—a surface layer velocity scale which characterizes surface momentum flux, and Ψ_h an integrated Monin-Obukhov (M-O) stability-correction factor for sensible heat (Section S2.3)—an empirical function of the dimensionless ratio $(z-d)\,/\,L$ where L is the M–O length (Monin and Obukhov, 1954). Both z_o and d are fit parameters to the logarithmic wind profile under neutral stability (Monin and Obukhov, 1954). Empirical values typical of natural vegetated surfaces are: $z_o \sim 1/10$ canopy height (h_c) and $d \sim 2/3\ h_c$ (Garratt, 1992; Oke, 1987). At heights well above the surface ($z > 10\ h_c$), d may be ignored in the calculation of R_a (Garratt, 1992), as is done in GEOS-Chem since dry deposition is referenced from surface grid box centers ($z \sim 60$ m AGL). Equation (S1) applies equally to all trace gas and aerosol species and assumes equivalency in the turbulent transfer of momentum and scalers under neutral conditions from z to z_o. It is noted that R_a according to Eq. (S1) assumes a 'no-slip' boundary condition, that is, $u(z_o) = 0$ m s^{-1}—the implications of which are discussed in Sections 3.1 & S2.4.

Across the distance z_o, molecular diffusion becomes an important factor governing near-surface trace gas flux. The species-specific quasi-laminar boundary layer resistance accounts for the transfer of gases from z_o to the deposition surface, and is estimated using the semi-empirical formulation of Wesely and Hicks (1977):

$$R_b(x) = \frac{2}{ku_*}\left(\frac{\kappa}{D_x}\right)^{2/3}, \quad \text{(S2)}$$

where κ is the thermal diffusivity of air and D_x the molecular diffusivity of the depositing trace gas x. Developments made herein to the calculation of D_x from GEOS-Chem are discussed in Section 3.2.

The resistance to surface uptake of trace gases in GEOS-Chem is parameterized according to a modified 'big-leaf' algorithm based on the W89 scheme, as is currently the case for the majority of global CTMs (Hardacre et al., 2015). Species-specific bulk-canopy surface resistance $R_c(x)$ is computed as multiple deposition pathways acting in parallel, including to: (i) upper canopy leaf interiors via stomatal r_s and mesophyll r_m resistances, (ii) upper canopy leaf cuticles r_{lu}, (iii) lower canopy elements $r_{dc} + r_{cl}$, and (iv) ground surface elements $r_{ac} + r_{gc}$:

$$R_c(x) = \left[1/(r_s + r_m) + 1/r_{lu} + 1/(r_{dc} + r_{cl}) + 1/\left(r_{ac} + r_{gc}\right)\right]^{-1}, \quad \text{(S3)}$$

The W89 algorithm was originally developed over the U.S. and southern Canada for use on 11 land types, with component resistances varying across 5 seasonal categories (summer, autumn, late autumn, winter, spring). Application to a variety of trace gases was made possible by r_s dependence on molecular diffusivity and r_m, r_{lu}, r_{cl}, and r_{gc} dependence on (i) aqueous solubility at neutral pH via effective Henry's solubility (H^*) and (ii) oxidative capacity via an estimated reactivity factor (f_o) categorized as

unreactive ($f_o = 0$), slightly reactive ($f_o = 0.1$), or as reactive as O_3 ($f_o = 1$). Categorized f_o values are based on electron activities and rate-of-reaction with aqueous S(IV) compounds (Wesely, 1989). In-canopy aerodynamic resistance to turbulent transport to the lower canopy and ground surface is represented by land type dependent fixed values r_{dc} and r_{ac}, respectively. Implementation of the W89 algorithm into GEOS-Chem included modifications for application to the global scale (Wang et al., 1998). Detailed descriptions of these modifications have been included in recent work evaluating the dry deposition of O_3 in GEOS-Chem (Silva and Heald, 2018; Wong et al., 2019) and can be found online, along with the fixed input parameters used in Eq. (S3) for the calculation of $R_c(x)$, at http://wiki.seas.harvard.edu/geos-chem/index.php/Dry_deposition (last accessed on 19/04/2025). Following the recommendations of Shah et al. (2018), we limit the cold temperature exponential increase in the non-stomatal components of R_c to a factor of 2 and impose a nominally small $R_c(HNO_3) = 1$ s m^{-1}.

Meteorological inputs to the parameterization of V_d in GEOS-Chem are provided from assimilated meteorological fields from NASA's Global Modeling and Assimilation Office (GMAO). Daily LAI values are interpolated from a gridded MODIS-derived monthly LAI product (Myneni et al., 2002). For this study, we have implemented the option to use on-site meteorology and canopy characterizations to drive the GEOS-Chem dry deposition scheme in single-point-mode.

S2 Aerodynamic resistance in the surface layer

S2.1 Aerodynamic resistance over Harvard Forest

Turbulent vertical transport of scalars within the atmospheric surface layer, often described as the lowest 10 % of the planetary boundary layer where fluxes of momentum, heat, and mass are assumed to be constant with height, is an important process governing surface-atmosphere exchange. Aerodynamic resistance to turbulent transport, most commonly parameterized in CTMs following Eq. (S1), can take on a large range of values depending on the state of surface layer turbulence. Cumulative distributions of hourly values of R_a computed over Harvard Forest (June–November 2000) following parameterizations P1–P3 using MERRA-2 assimilated meteorology are depicted in Fig. S1 for two reference heights, 29 m and 60 m. Also depicted is R_a inferred from measured horizontal wind and friction velocity (u_*) at 29 m, $R_a(29m) = u$ (29 m)/ u_*^2, assuming a no-slip boundary condition, i.e., $u(z_o) = 0$ m s^{-1}. Computed from the center of the lowest level in GEOS-Chem, P1 $R_a(60\ m)$ ranges from ~ 6 s m^{-1} (5th percentile) to ~ 400 s m^{-1} (95th percentile) with 50th percentile $R_a(60m)$ ~ 18 s m^{-1}. Thus, R_a has variable influence to total resistance represented through V_d, ranging from minor under well mixed conditions for species with substantial R_c, i.e., O_3 (Massman et al., 1994), HCN (Nguyen et al., 2015), and NO_2 (herein), to significant for species with negligible R_c under typical diabatic conditions, i.e., HNO_3 (herein), to dominant under conditions of very high stability and intermittent turbulence (Toyota et al., 2016).

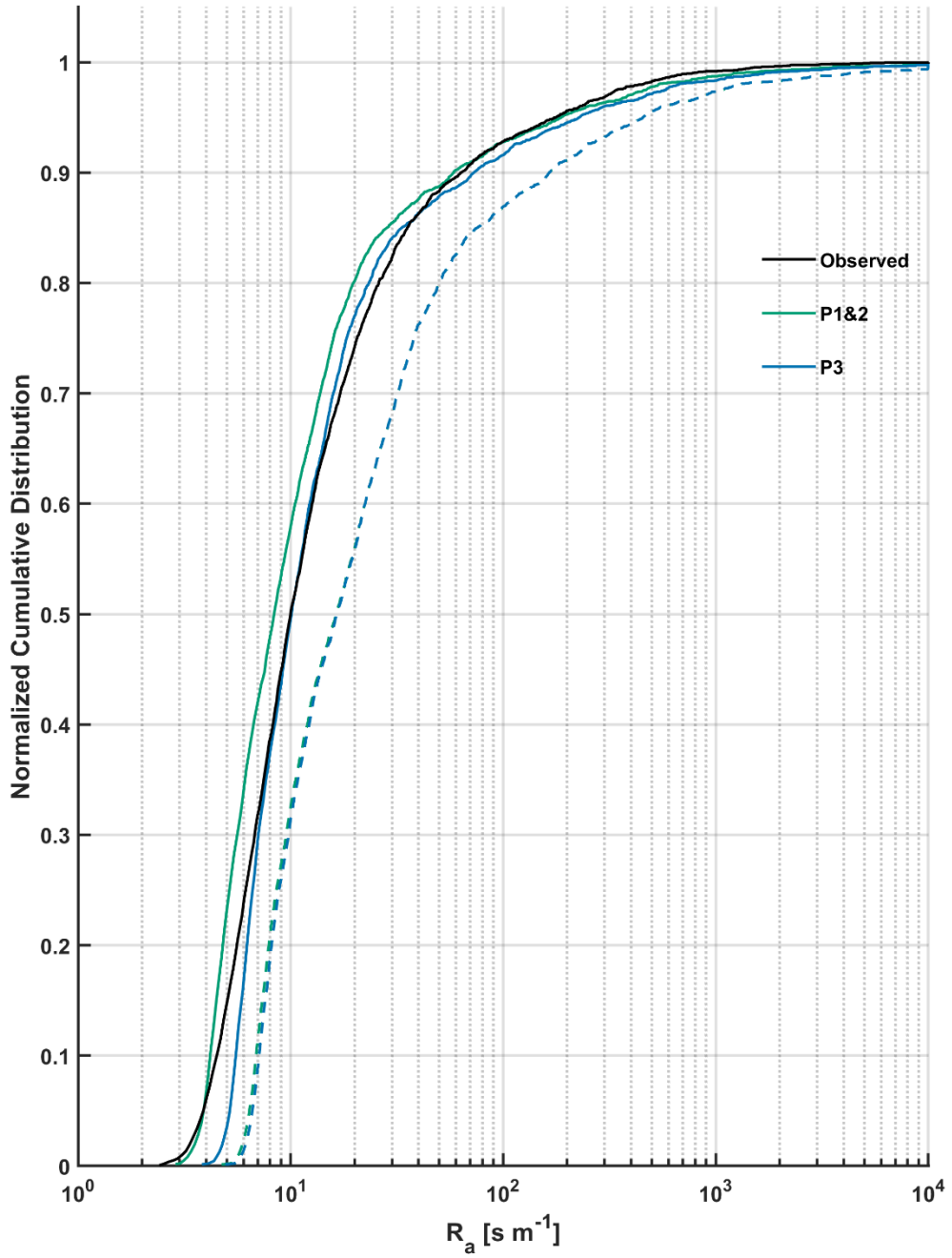

Figure S1: Cumulative distributions of hourly aerodynamic resistance R_a over Harvard Forest from June–November 2000. Measurement-inferred $R_a(29\ m) = u(29\ m)/u_*^2$ is compared to coincidently sampled (hourly) simulated values P1&2 and P3 integrated from both the 29 m measurement height at Harvard Forest (**solid lines**) and the approximate midpoint of GEOS-Chem's first level, ~ 60 m (**dashed lines**).

S2.2 Formulation of R_a from eddy diffusivity K_c

An equivalent formulation of R_a to that of Eq. (S1) may be expressed as a vertical integration of eddy diffusivity K_c (Garratt, 1992):

$$R_a = \int_{z_o}^{z-d} \frac{1}{K_c(z)}\, dz\,, \qquad \text{(S4)}$$

K_c is the eddy diffusivity for scalar quantities which is commonly represented as the product of characteristic surface layer scaling parameters u_* and height z above the displacement height (d) (Kaimal and Finnigan, 1994), corrected for non-neutral conditions

via an empirically determined dimensionless flux–gradient relation for sensible heat ϕ_h commonly used interchangeably for scalar quantities:

$$K_c = \frac{u_* k(z-d)}{\phi_h(\zeta)}, \quad \text{(S5)}$$

where k = 0.4 is the von Karman constant, ϕ_h is an empirical function of the dimensionless M–O stability parameter $\zeta = (z - d) / L$, where L is the M–O length (Monin and Obukhov, 1954). Figure S2 includes calculated values of K_c following Eq. (S5), integrand of Eq. (S4) K_c^{-1}, and resulting R_a following Eq. (S4) as a function of height above ground over a rough surface under neutrally stable conditions.

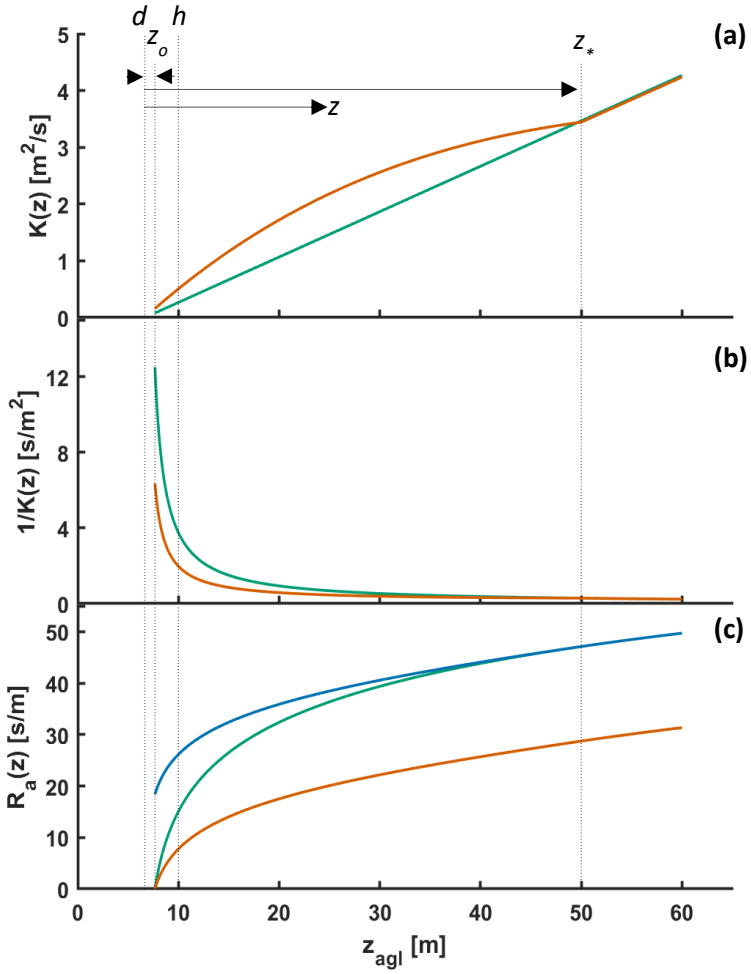

Figure S2: (a) Turbulent eddy diffusivity *K(z)* above a rough surface (z_o = 1 m) computed via standard Monin–Obukhov similarity theory according to Eq. (S5) (**green**) and using a perturbed Monin–Obukhov form (Eq. (S11)) to account for enhanced mixing within the roughness sublayer (**orange**). **(b)** $K(z)^{-1}$ depicts the integrand of corresponding aerodynamic resistance calculations (Eq. (S4)). **(c)** Aerodynamic resistance $R_a(z)$ computed following Eq. (S4) with stability correction functions according to M–O similarity theory (**green**) and a roughness sublayer perturbed from (Eq. (S11)) (**orange**), both of which assume zero wind at the roughness length z_o. $R_a(z)$ which accounts for both enhanced roughness sublayer mixing and non-zero wind at z_o is depicted in **blue** according to Eq. (S13). Meteorological conditions are taken as light winds (u_* = 0.2 m s^{-1}) and a neutrally stable atmosphere (L^{-1} ~ 0 m^{-1}).

S2.3 Monin–Obukhov (M–O) stability correction functions used in GEOS-Chem

Empirically determined dimensionless flux–gradient relations, also known as M–O stability correction functions, used to compute surface layer R_a in GEOS-Chem have the following functional (ϕ_h) and integral (Ψ_h) forms:

Unstable conditions ($\zeta < 0$) (Garratt, 1992; Holtslag et al., 1990)

$$\phi_h = (1 - 15\,\zeta)^{-1/2}\,, \tag{S6}$$

$$\Psi_h = 2\ln\left[\frac{1+\phi_h^{-1}}{2}\right], \tag{S7}$$

Stable conditions ($0 < \zeta \leq 1$) (Dyer, 1974)

$$\phi_h = 1 + 5\zeta\,, \tag{S8}$$

Stable conditions ($\zeta > 1$) (Holtslag et al., 1990)

$$\phi_h = 5 + \zeta\,, \tag{S9}$$

Stable conditions ($\zeta > 0$) (Holtslag and Bruin, 1988)

$$\Psi_h = -\left[a\zeta + b\left(\zeta - \frac{c}{d}\right)e^{-d\,\zeta} + \frac{bc}{d}\right], \tag{S10}$$

where a = 0.7, b = 0.75, c = 5, and d = 0.35.

S2.4 Roughness sublayer (RSL) mixing

Within a distance of 2 to 3 times the canopy height (h_c) above the surface, the so called roughness sublayer (RSL), turbulent eddy structure is significantly different from that of the remaining surface layer above (Finnigan et al., 2009; Raupach et al., 1996). Turbulent flows in the wake of roughness elements are dominated by structures of a larger length scale than predicted by Eq. (S5) where turbulent eddies are parameterized to scale on a distance z above d (Finnigan, 2000). Near the canopy top, K_c is enhanced over that predicted by M–O similarity theory by a factor of 2 to 3 (Cellier and Brunet, 1992; Raupach et al., 1996), approaching equivalence by ~ $2h_c$ (Simpson et al., 1998). To avoid underestimating turbulent transport of momentum, heat, and mass, models that employ gradient transport theory (K-theory) may scale eddy diffusivities within the RSL to values above those predicted by M–O similarity theory (Bryan et al., 2012; Mölder et al., 1999; Neirynck and Ceulemans, 2008; Sellers et al., 1986; Stroud et al., 2005). RSL functions $\widehat{\phi_x}$ designed as perturbations to the dimensionless universal M–O functions $\phi_x(\zeta)$ can be applied in multiplicative form, yielding modified M–O stability functions Φ_x:

$$\Phi_x = \phi_x(\zeta)\,\widehat{\phi_x}\,, \tag{S11}$$

where x refers to either momentum, heat, or scalar quantities. Several RSL functional forms have been proposed of varying complexity, all of which contain an additional RSL length scale, i.e., z^* in Eq. (S12). Computing mean wind and scalar profiles requires integral forms of corresponding non-dimensional M–O stability functions (Panofsky, 1963); some RSL modified M–O stability functions have analytical solutions to integral forms (Arnqvist and Bergström, 2015; de Ridder, 2010), while others require numerical integration (Cellier and Brunet, 1992; Garratt, 1980; Harman and Finnigan, 2007; Mölder et al., 1999; Wenzel et al., 1997). Physick and Garratt (1995) implement a simple RSL lower boundary correction into a mesoscale model using the RSL function:

$$\widehat{\phi_M} = \widehat{\phi_h} = 0.5\,\exp\left[0.7\,\frac{(z-d)}{(z^*-d)}\right], \tag{S12}$$

where the RSL correction is treated the same for both momentum $\widehat{\phi_M}$ and sensible heat $\widehat{\phi_h}$ and is independent of buoyancy. Following Eq. (S12), turbulent mixing within the upper canopy at d is enhanced 2-fold, with $\widehat{\phi_M}$ and $\widehat{\phi_h}$ decaying to unity at the top of the RSL, z^*. The depth of the RSL was estimated following Physick and Garratt (1995); briefly, for neutral and unstable

conditions ($L^{-1} \leq 0$), $z_N^* = 50\ z_o$; for very stable conditions ($z_N^* / L > 0.2$), $z^* = 0.37\ z_N^*$; for moderately stable conditions ($0 < z_N^* / L < 0.2$), z^* is linearly interpolated between neutral and stable values. It is noted that the additional mixing in the wake of roughness elements within the RSL reduces vertical gradients from those of M–O adjusted logarithmic values extrapolated from above the RSL; as such, flux–gradient wind profiles adjusted for stability and RSL effects can no longer be integrated assuming $u(z_o) = 0$ for $z < z^*$. An updated formulation of R_a which accounts for RSL effects and $u(z_o) > 0$ can be expressed as (Physick and Garratt, 1995):

$$R_a(z < z^*) = \frac{1}{ku_*}\left[\ln\left(\frac{z-d}{z_o}\right) - \Psi_h\left(\frac{z-d}{L}\right) + \Psi_h\left(\frac{z_o}{L}\right) + \int_z^{z^*} \phi_h\left(1 - \widehat{\phi_h}\right)z^{-1}dz\right], \quad \text{(S13)}$$

At the top of the RSL where $z = z^*$ and $\widehat{\phi_h} \sim 1$, R_a from Eq. (S1) & Eq. (S13) become equivalent. Above the RSL ($z > z^*$) M–O similarity theory applies and R_a follows Eq. (S1).

Included in Fig. S2 is a depiction of the effects of enhanced RSL mixing on K_c and R_a as a function of reference height z above the displacement height d for a rough surface ($z_o = 1$ m) under neutral stability conditions ($L^{-1} \sim 0$) and light winds ($u_* = 0.2$ m s^{-1}). K_c and K_c^{-1} calculated using the RSL modified M–O stability function Φ_x from Eq. (S12) are shown as orange traces in panels (a) and (b) of Fig. S2, respectively, and are compared to values from M–O similarity theory which neglects RSL effects (green trace). The largest relative difference in RSL-corrected K_c occurs at z_o, where the effect of Eq. (S12) is largest. Panel (c) in Fig. S2 includes $R_a(z)$ computed following M–O similarity theory (Eq. (S1), green trace) alongside $R_a(z)$ according to Eq. (S13) (blue trace); the integral in Eq. (S13) was evaluated numerically via Simpson's method. Enhanced RSL mixing results in a weaker above-canopy vertical gradient in R_a, while allowing $u(z_o) > 0$ via Eq. (S13) results in a large displacement of $R_a(z_o)$. R_a following Eq. (S1) and Eq. (S13) asymptotically converge to equivalency by $z = z^*$, with good and excellent agreement by $z = 2h_c$ (10 %) and $z = 3h_c$ (3 %), respectively, under these neutral test conditions. Reduced gradients in R_a with height results from growth of turbulent eddies (K_c) according to mixing length z - d. As previously noted, R_a computed from integration of K_c^{-1} (Eq. (S5)) where K_c is corrected for buoyancy following ϕ_h is equivalent to R_a computed following Eq. (S1), both being depicted in panel (c) of Fig. S2 (green trace). However, integration of K_c^{-1} where K_c is corrected for buoyancy and RSL effects following the modified M–O stability correction $\widehat{\phi_h}$ is not equivalent to RSL R_a computed following Eq. (S13), as seen in Fig. S2c (orange trace), as the former assumes $u(z_o) = 0$ and the later $u(z_o) > 0$. Although the vertical gradients of these two methods are identical, R_a corrected for the RSL following Eq. (S13) is shifted by $R_a(z_o)$.

It is noted that RSL-corrected R_a has directional asymmetry, where aerodynamic resistance to upward transport of surface emissions (orange trace in Fig. S2) is significantly less than aerodynamic resistance to dry deposition (blue trace in Fig. S2). This directional asymmetry is intuitive, as resistance to upward mixing of surface emissions would not be impeded, but enhanced, by non-zero wind at z_o, whereas dry deposition of uniformly mixed trace species from aloft requires contact with surface elements for removal. It is also noted that many efforts to simulate bidirectional surface exchange of atmospheric trace species employ R_a following standard M–O similarity theory according to Eq. (S1) for both emission and deposition pathways (Haghighi and Or, 2015; Karamchandani et al., 2015; Nemitz et al., 2000; Su et al., 2011; Wen et al., 2014; Wentworth et al., 2014), thus failing to account for directional asymmetry in resulting fluxes. To prevent the underestimation of upward sensible and latent heat fluxes, Sellers et al. (1986) in their formulation of a Simple Biosphere Model (SiB) for use in General Circulation Models (GCMs) impose an aerodynamic resistance to emission from an integration of a RSL modified K_h, which would be similar to that depicted in Fig. S2c (orange trace). In Boys et al. (in prep), directional asymmetry of R_a is implemented into a simple model of subgrid dry deposition of near-surface emitted NO_x.

S3 Review of reactive uptake coefficients for NO_2 to hydrated surfaces

Although the mechanism for heterogenous hydrolysis of NO_2 (reaction R1 in main text), likely involving disproportionation of N_2O_4 as a surface intermediate (Finlayson-Pitts et al., 2003), is still an active area of research (Bang et al., 2015; Finlayson-Pitts, 2009; Murdachaew et al., 2013; Spataro and Ianniello, 2014), uptake coefficients for NO_2 (γ_{NO_2}) to various surfaces have been measured. Laboratory determined values of γ_{NO_2} are generally in the range of 10^{-7} to 10^{-5} for humidified and aqueous surfaces of various composition (Ammann et al., 2005; Bröske et al., 2003; Kleffmann et al., 1998; Kurtenbach et al., 2001), however, values > 10^{-5} (Mertes and Wahner, 1995; Msibi et al., 1993) and < 10^{-8} (Ammann et al., 2013) to bulk liquid water have been reported. Studies finding slow uptake of NO_2 to bulk water understand the process as driven by low solubility and slow aqueous phase second-order hydrolysis (Cheung et al., 2000; Lee and Schwartz, 1981; Schwartz and Lee, 1995), while studies finding uptake above that which can be accounted for by these solution-phase processes suggest heterogeneous first-order hydrolysis at the air–water interface (Bambauer et al., 1994; Finlayson-Pitts et al., 2003; Mertes and Wahner, 1995; Novakov, 1995). Recent efforts to understand the orders of magnitude variation in laboratory determined γ_{NO_2} to aqueous surfaces have used electrospray ionization (ESI) mass spectrometry (MS) to monitor online NO_3^- formation from the reaction of $NO_{2(g)}$ injected into the ESI source region with aqueous electrosprays containing various concentrations of atmospherically relevant solutes, finding large enhancements in inferred γ_{NO_2} of up to a factor of 10^4 to solutions containing halide salts NaX (X = Cl, Br, I) (Colussi and Enami, 2019; Kinugawa et al., 2011; Yabushita et al., 2009). It was proposed that interfacial anions (Cl^-, Br^-, I^-) stabilize NO_2 at the air–water interface, facilitating heterogeneous hydrolysis. To this end, it was noted that Bambauer et al. (1994) reported enhanced uptake of NO_2 to aqueous droplets containing ~ 3 mM NaCl; however, Msibi et al. (1993) reported a value for γ_{NO_2} to deionized water of 8.7 x 10^{-5} at ~ 0.6 ppm NO_2—much greater than can be accounted for by dissolution followed by second-order hydrolysis, i.e., γ_{NO_2}~ 6 x 10^{-9} at 10 ppb NO_2 (Ammann et al., 2013). Due to the unique complexity of the ESI process, further work is required before application of these results to atmospherically relevant interfacial surfaces (Gallo et al., 2019b, 2019a; Rovelli et al., 2020). Additionally, the presence of reducing solutes such as ascorbic acid (Msibi et al., 1993) and phenolic humic acid precursor molecules (Ammann et al., 2005) have been shown to significantly enhance NO_2 surface uptake via one-electron reduction reactions yielding HONO/nitrite, and may also contribute to NO_2 deposition within the interior of leaves (Farvardin et al., 2020).

For use in models of atmospheric chemistry, field–measured γ_{NO_2} have provided some constraint on the large variation in laboratory determined values. Kurtenbach et al. (2001) studied heterogeneous HONO formation in a road traffic tunnel in Wuppertal, Germany, and found γ_{NO_2} ~ 10^{-6} to a sample of tunnel wall residue to be in good agreement with first-order heterogeneous formation rates of HONO from the tunnel experiments. VandenBoer et al. (2013) report high resolution vertical profiles (10 m resolution to 250 m AGL; < 10 min/profile) of various trace species including HONO and NO_2 at the Boulder Atmospheric Observatory (BAO) in Colorado, U.S. during late winter of 2011. The BAO site was situated in an agricultural region 32 km northeast of Boulder and was decommissioned in 2018 (Wolfe and Lataitis, 2018). VandenBoer et al. (2013) derived ground uptake coefficients for NO_2 ($\gamma_{NO_2,\ ground}$) by assuming the column-integrated rate of change of HONO during the first half of the night (1800–2400) when HONO was increasing from very low daytime concentrations (mid-day photolysis lifetime of HONO < 15 minutes) was due to heterogeneous hydrolysis of NO_2 occurring on ground surfaces, and found $\gamma_{NO_2,\ ground}$ to vary between 2 x 10^{-6} and 1.6 x 10^{-5} as a function of RH for the specific wintertime land type in the vicinity of the BAO site (grassland and tilled fields). Ren et al. (2020) monitored NO_2 and HONO concentrations at high temporal resolution at a meadow location (grass height ~ 30 cm, LAI ~ 6) in Melpitz, Germany, and similarly compute NO_2 uptake coefficients due tos reaction R1 during early evening when HONO is accumulating in the nocturnal boundary layer, finding γ_{NO_2} = 2.3 ± 1.9 x 10^{-6}. Collins et al. (2018) found γ_{NO_2}=

(1–2.3) x 10^{-6} from NO_2 decay, presumably via reaction R1, following indoor (residential) perturbation experiments probing the gas–surface equilibrium control over HONO concentrations for which surfaces have developed sufficient reservoirs of HONO/nitrite via heterogeneous reaction of NO_2 and by deposition of HONO emitted during operation of a gas stove.

S4 Parameterization of soil NO canopy reduction factor (CRF) in GEOS-Chem

Within-canopy NO_x loss processes removing up to 70–80 % of soil-emitted NO in mature forest ecosystems have been required to reconcile measured soil NO emissions with above-canopy NO_x observations (Jacob and Wofsy, 1990; Lerdau et al., 2000; Min et al., 2014). Emitted from soils as NO and deposited within canopies as NO_2, deposition-based parameterizations of soil NO canopy reduction factors (CRF) for use in large-scale CTMs yield global mean reductions in above-canopy soil NO_x fluxes from ~ 20 % (Wang et al., 1998) to 50 % (Yienger and Levy II, 1995). Soil NO in GEOS-Chem follows the Berkeley–Dalhousie Soil NO_x Parameterization (Hudman et al., 2012), with a CRF as implemented by Wang et al. (1998):

$$CRF = \frac{k_d}{k_v + k_d}, \tag{S14}$$

where k_v [m s^{-1}] is the canopy air ventilation coefficient (Martens et al., 2004; Trumbore et al., 1990) and k_d [m s^{-1}] the deposition coefficient for NO_2 in canopy air. k_v is an empirical function of land type, surface wind speed, and LAI and is tuned to yield canopy air residence times for soil-emitted inert tracers in the Amazon Rainforest of 1 h during daytime and 5 h at night (Jacob and Wofsy, 1990). Nocturnal canopy air residence times on the order of 2–10 h for the Amazon Rainforest have been estimated from in-canopy measurements of soil-emitted ^{222}Rn (Martens et al., 2004; Trumbore et al., 1990). Application of k_v to additional land types in GEOS-Chem follows:

$$k_v = k_v^{RF} \sqrt{\frac{u^2}{9} \frac{7}{LAI}} \frac{\gamma^{RF}}{\gamma}, \tag{S15}$$

where u is the wind speed 10 m above the displacement height, k_v^{RF} is the canopy air ventilation coefficient tuned for the Amazon Rainforest (LAI = 7, u = 3 m s^{-1}) with daytime and nighttime values of 1x10^{-2} m s^{-1} and 2x10^{-3} m s^{-1}, respectively, and γ a nondimensional extinction coefficient for in-canopy wind speed with a value of 4 for both rainforest and temperate forest ecosystems (Wang et al., 1998). The deposition coefficient k_d in GEOS-Chem is taken as $R_c(NO_2)^{-1}$. Hudman et al. (2012) find that this representation of the CRF in GEOS-Chem results in a 16 % global reduction in above-canopy soil NO emission. Herein, we compute the CRF following Eqs. (S14–S15) using site specific meteorology and canopy parameters. We set $k_d = [(R_c(NO_2)^{-1} + R_{chem}(NO_2 \rightarrow N_2O_5)^{-1}]$, where in addition to canopy uptake as described through $R_c(NO_2)$, we include an estimate of the minimum canopy resistance to nocturnal chemical loss of NO_2, $R_{chem}(NO_2 \rightarrow N_2O_5) = V_{chem}^{-1} \sim 2000$ s m^{-1}. We note that k_d following this approach assumes that soil NO is oxidized to NO_2 on a much shorter timescale (minutes) than nocturnal vertical mixing of ground-level air parcels—a reasonable assumption given that: (i) nocturnal in-canopy O_3 concentrations of 10–25 ppb are much greater than NO concentrations at this site (Horii et al., 2004; Munger et al., 1996) and (ii) air parcel residence times for stable evening/nighttime conditions are on the order of tens of minutes to hours in the lower canopy of mature forests (Bannister et al., 2023; Martens et al., 2004; Trumbore et al., 1990). Recent observations of daytime air parcel residence times in mature forest canopies are on the order of tens of seconds to a few minutes (Bannister et al., 2023; Martens et al., 2004)—much less than 1 h to which daytime k_v^{RF} in Eq. (S15) is tuned. Although beyond the scope of this work, updating the parameterization of k_v in GEOS-Chem to yield more realistic daytime canopy air residence times (Gerken et al., 2017) seems warranted. Such reductions in simulated daytime canopy air residence times would result in commensurate reductions to the CRF in Eq. (S14) due

to reduced time for deposition of NO_2 prior to ventilation; however, incorporation of canopy NO_x chemistry into the CRF parameterization could partially offset these reductions (Delaria and Cohen, 2020; Min et al., 2014). Given the nocturnal focus of this study, we proceed with using the CRF parameterization from GEOS-Chem, modified to include nocturnal chemical loss of NO_2 in addition to deposition, as previously discussed.

As seen in the bottom panel of Fig. S3, the CRF from the base simulation P1 results in canopy-top soil NO reductions of 30 % at night, increasing slightly to 35 % during the day at the location of Harvard Forest over the period April–November. This weak diel behavior results from a similar day-to-night reduction in both k_d and k_v of more than an order of magnitude (Fig. S8 includes diel $R_c(NO_2)$ at the HFEMS). The reversal of the CRF diel pattern seen in updated parameterizations P6–P8 reflect the large increases in simulated surface uptake of NO_2 at night through implementation of reaction R1 via dry deposition, discussed in Section 3.3.3.

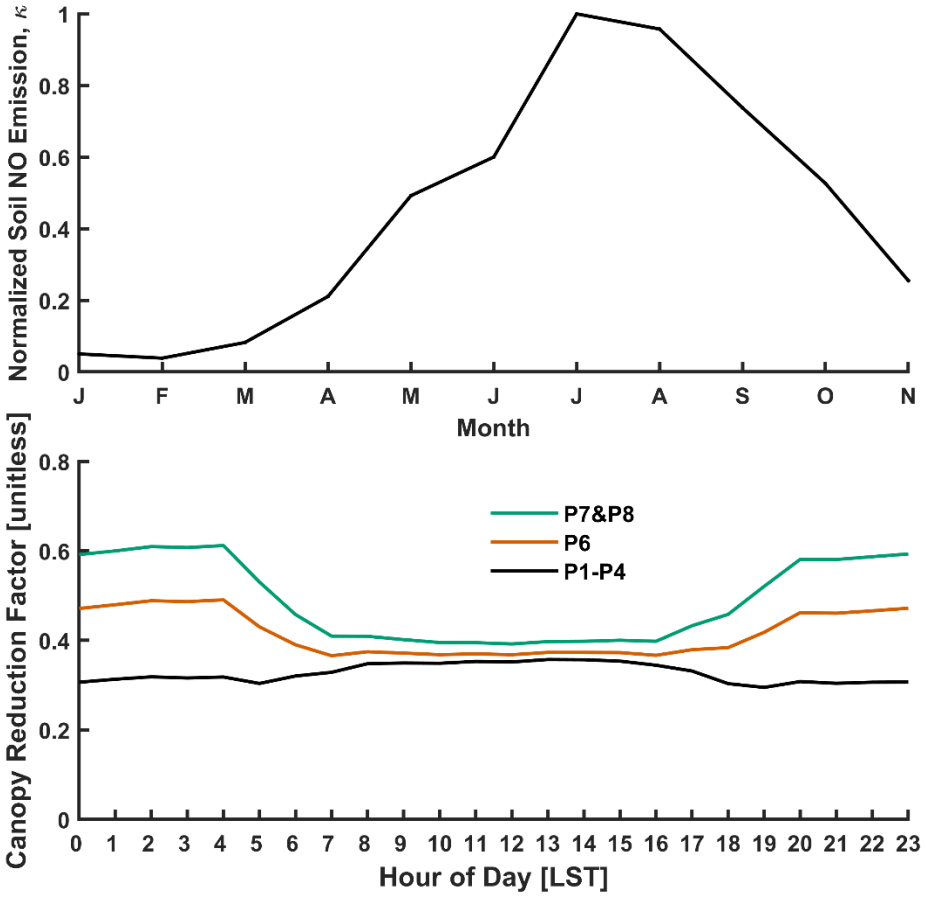

Figure S3: (**TOP**) Normalized monthly nocturnal soil NO emission simulated from GEOS-Chem at the location of Harvard Forest. (**BOTTOM**) Diel climatology (April, July–November) of the soil NO canopy reduction factor (Eq. (S14)) for parameterizations P1–P4, P6, and P7 & P8.

S5 Simulated diel profiles of $V_d(x)$ for measured NO_y component species

Figure S4 depicts simulated diel mean deposition velocities from selected updated parameterizations for NO_y component species HNO_3, PAN, and NO_2 over Harvard Forest, aggregated from hourly values computed using observed meteorology and canopy characteristics. Corresponding simulated component resistances R_a, R_b, and R_c are depicted in Fig. S8. Unless otherwise indicated, aerodynamic resistance was computed from the measurement height of 29 m. Depicted simulations of $V_d(HNO_3)$ include parameterizations P2 (equivalent to P1 referenced from measurement height; Table 2), P3 (RSL correction assuming $u(z_o) > 0$ m s^{-1}), P4 (improved calculation of molecular diffusivity), and P8 referenced from both the measurement height (29 m) and the center of GEOS-Chem's lowest grid box (~ 60 m). The computation of $V_d(HNO_3)$ between parameterizations P4 and P8 is equivalent, i.e., identical formulations of R_a and R_b (Table 2). The small increase in daytime R_a of ~ 15 % due to the incorporation of the RSL in parameterization P3 (Fig. S8) results in a small (~ 7 %), yet significant ($p < 0.05$), decrease in daytime $V_d(HNO_3)$ compared to P2 values—a slightly greater change than observed over Talladega National Forest (Section 3.1, Table 3) where a higher relative measurement height (2 h_c vs. 1.5 h_c at Harvard Forest) dampened the effect of the RSL on R_a computed from this altitude. Similarly, the lower depth of influence of the RSL during nocturnal conditions results in P3 updates having a reduced effect on nighttime $V_d(HNO_3)$. Due to low aqueous solubility of NO_2 and PAN, R_c is the dominant term in the resistance pathway for these species (Fig. S8) outside of infrequent very stable conditions (Fig. S1); accordingly, RSL corrections to R_a in parameterization P3 have negligible influence on resulting deposition velocities for these species. Large reductions in simulated $V_d(HNO_3)$ are seen for parameterization P4, where the use of accurate molecular diffusivities results in an increase in $R_b(HNO_3)$ of ~ 95 %. Associated increases in $R_b(NO_2)$ and $R_b(PAN)$ of ~ 60 % and 110 %, respectively, result in insignificant reductions to $V_d(NO_2)$ across all times of day and small reductions in daytime $V_d(PAN)$ of 7 % due to the dominant contributions of R_c for these species. However, due to the dependence of species-specific stomatal conductance on the ratio of molecular diffusivities D_x/D_{H_2O}, diffusivity updates to parameterization P4 result in increased stomatal resistances with notable reductions in daytime dry deposition for species that deposit under stomatal control—up to 13 % and 32 % for NO_2 and PAN, respectively. At night when stomates are assumed to be closed ($r_s > 10^4$ s m^{-1}), non-stomatal branches of R_c control deposition, therefore reducing the effects of updates to molecular diffusivity on the nocturnal dry deposition of NO_2 and PAN as depicted in Fig. S4.

Included in Fig. S4 for simulated $V_d(NO_2)$ is the effect of replacing the non-stomatal branch of R_c with r_{hyd} according to Eq. (8), resulting in large increases in nocturnal $V_d(NO_2)$ of up to a factor of 6, as depicted in parameterizations P6 & P8. The relative increase in daytime $V_d(NO_2)$ is much less (24% for P8 with $\alpha = 2$) due to competing stomatal uptake, however, enough to restore peak daytime $V_d(NO_2)$ to base levels. The reduced diel variability in simulated $V_d(NO_2)$ seen for parameterization P8, ~ 4-fold compared to 20-fold for P2, is consistent with the diurnal cycles in $V_d(NO_2)$ inferred from canopy-scale observations where daytime values are on the order of 2 to 7 times greater than at night (Eugster and Hesterberg, 1996; Hanson and Linderg, 1991; Plake et al., 2015; Rondón et al., 1993; Stella et al., 2013; Walton et al., 1997). Greater diurnal variation in $V_d(NO_2)$ is seen in leaf-level uptake studies, where daytime deposition velocities are on average an order of magnitude greater than in the absence of photosynthetically active radiation (Delaria et al., 2018, 2020).

Turnipseed et al. (2006) present eddy covariance flux observations of PAN over a summertime coniferous forest in North Carolina, finding appreciable nocturnal dry deposition that increases when the canopy is wet—well-above predicted values from the W89 scheme. Accordingly, parameterization P8 includes suggested empirical updates for dry deposition of PAN developed by Turnipseed et al. (2006) for forested ecosystems, namely, setting non-stomatal resistance to cuticular deposition (r_{lu} in Eq. (S3)) to 250 s m^{-1} for dry foliage and 125 s m^{-1} for wet foliage. Turnipseed et al. (2006) define leaf surfaces as wet during and immediately

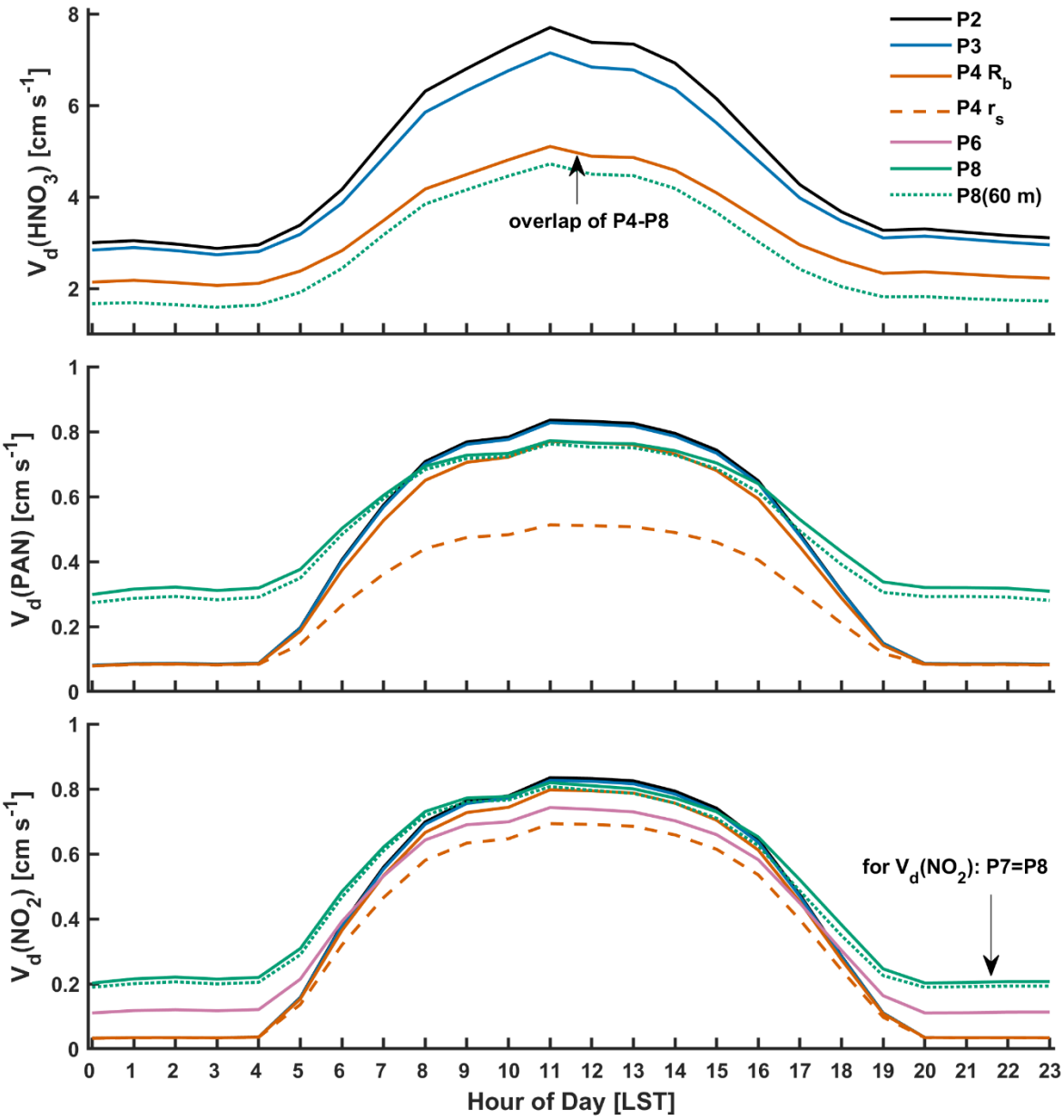

Figure S4: Simulated diel mean deposition velocities for HNO_3, PAN, and NO_2 over Harvard Forest (June–November). In addition to depicted parameterizations from Table 2, shown for parameterization P4 is the cumulative effect of molecular diffusivity updates to quasi-laminar sublayer resistance R_b followed by resistance to stomatal uptake r_s, observable for daytime PAN and NO_2 which deposit under stomatal control. Simulated deposition velocities were computed from the measurement reference height of 29 m, unless otherwise indicated (i.e., P8(60 m)). Diel mean values are from a continuous hourly dataset computed using observed meteorological and canopy-specific (LAI, canopy height) inputs. Component resistances R_a, R_b, and R_c are shown in Fig. S8.

following precipitation events or when above-canopy RH > 96 %; herein, for the purposes of computing $V_d(PAN)$, we define the canopy as wet when above-canopy RH > 96 %. To extend applicability to other forest locations, we scale recommended cuticular resistances by the ratio LAI_{HFEMS} / 3.5, where 3.5 m^2 m^{-2} was the LAI at the study site of Turnipseed et al. (2006). This update to non-stomatal uptake of PAN in parameterization P8 reduces median nocturnal $R_c(PAN)$ over Harvard Forest from ~ 1000 s m^{-1} to 200 s m^{-1} (Fig. S8), resulting in nocturnal and daytime increases to $V_d(PAN)$ of 250 % and 60 %, respectively (Fig. S4). As was seen with updates to $V_d(NO_2)$ in Fig. S4, parameterization P8 updates to $V_d(PAN)$ largely restore reduced daytime values in parameterization P4 to P2 base levels. It is noted that the empirical update from Turnipseed et al. (2006) is not mechanistically based, nor is it clear as to the general applicability to other land types, locations, or seasons. As is often the case in parameterizations

of dry deposition processes, further study is warranted. Recent chamber studies of foliar uptake of PAN both question (Place et al., 2020) and support (Sun et al., 2016) the role of non-stomatal deposition, rendering dry deposition of PAN an active area of research.

Studies comparing CTM-simulated deposition velocities to measurement-inferred values often reference R_a from CTM grid-box-center instead of measurement heights (Clifton et al., 2017; Nguyen et al., 2015; Nowlan et al., 2014; Silva and Heald, 2018). Increases in R_a when referenced from the center of GEOS-Chem's lowest level (~ 60 m) instead of the 29 m measurement height over Harvard Forest results in moderate, although significant ($p < 0.05$), reductions in simulated $V_d(HNO_3)$ of 10 % (daytime) to 20 % (nighttime), as depicted in Fig. S4 by comparing parameterization P8 with P8(60m). These moderate increases in R_a are insufficient to cause significant change to either $V_d(PAN)$ or $V_d(NO_2)$ which deposit under R_c control.

S6 Review of nocturnal stomatal behavior

Stomatal pores exist in leaves to optimize plant water-use-efficiency—the number of molecules of H_2O transpired per molecule of CO_2 fixed via photosynthesis. Stomatal aperture is under guard cell regulation in response to environmental conditions such as solar radiation, guard cell CO_2 concentration, soil moisture, water vapor pressure deficit (VPD), and temperature (Costa et al., 2015; Nobel, 2009). Fully open stomata occupy ~ 0.2–2 % of leaf surface area, with a density of ~ 50–300 stomata per mm^2 on the stomata containing surfaces of leaves of temperate terrestrial plants, making available a moist interior leaf surface area to photosynthetic mesophyll cells that is in the range of 10–50 times larger than the projected leaf area (Nobel, 2009; Nobel et al., 1975).

Both canopy-scale and leaf-level observations of pollutant gaseous uptake attempt to separate stomatal from non-stomatal pathways. A simple approach is to assign nocturnal/dark uptake as entirely non-stomatal, dependent on the assumption of stomatal closure. In addition to darkness, chamber studies may introduce other stimuli known to reduce stomatal aperture, such as water stress, elevated CO_2, or the plant hormone abscisic acid (ABA) (Chaparro-Suarez et al., 2011; Costa et al., 2015; Delaria et al., 2020). Trace gas specific stomatal conductance (g_{sx}) may be deduced by scaling stomatal conductance to water vapor (g_s)—inferred in chamber studies by normalizing measured water vapor flux by leaf VPD (Delaria et al., 2020; Thoene et al., 1996; Wang et al., 2020), and in canopy-scale studies by inversion of the Penman–Monteith equation using above-canopy water vapor flux (Lamaud et al., 2009)—by the ratio of diffusivities D_x/D_{H_2O} in air. Estimates of stomatal conductance enable separation of non-stomatal from stomatal uptake—including estimates of mesophilic resistance to the leaf interior—by non-linear fits to plots of $V_d(x)$ vs g_{sx} (Delaria et al., 2020). However, this method assumes that the measured evaporative flux is due entirely to gaseous diffusion of water vapor through stomatal pores, without contribution from other sources including evaporation from soil or moisture that may be present on canopy elements as a result of precipitation, dew, or elevated humidity. Significant scatter and elevated values in inferred g_s have been noted at the canopy scale for RH > 60 % and for a period of time (days) following rainfall, motivating efforts to fit relations of g_s to CO_2 assimilation flux (which assume nocturnal stomatal closure) on ideal days for application across all conditions of canopy moisture (Lamaud et al., 2009; Plake et al., 2015; Stella et al., 2013).

In addition to the challenge of measuring stomatal conductance under elevated RH, mounting evidence exists for the presence of thin aqueous films on foliar surfaces at ambient humidities well below saturation, resulting from the deliquescence of deposited hygroscopic material in the high humidity laminar boundary layer of transpiring leaves (Burkhardt et al., 1999, 2001a; Burkhardt and Eiden, 1994; Burkhardt and Hunsche, 2013; Grantz et al., 2018). Concentrated solutions of deliquesced material have sufficiently low surface tension to spread over hydrophobic leaf cuticles and penetrate stomatal pores as thin liquid films (< 100 nm thick), connecting to apoplastic liquid water within the leaf interior—a process known as 'hydraulic activation of stomata' (HAS) (Burkhardt, 2010). An osmotic gradient in water potential drives water movement through hydraulically activated stomata

to the leaf exterior, where evaporation occurs uncoupled from stomatal aperture—a process known as 'wicking'. This additional pathway for water efflux escapes stomatal regulation, thereby reducing plant water-use-efficiency and drought tolerance. Significant increases in minimum cuticular conductance to water on the order of 23–30 % have been noted across coniferous and deciduous tree species for foliage exposed to ambient air (ionic aerosol concentration of 4.9 μg m^{-3}) compared to filtered air (ionic aerosol concentration of 0.67 μg m^{-3}) (Burkhardt et al., 2018). Similar experiments conducted on shorter lived faba beans (*Vicia faba*) noted significant increases in both minimum cuticular conductance (16 % average, 80 % max) and nocturnal stomatal conductance (~ 40 %) (Grantz et al., 2018). Foliar exposure studies to higher concentrations of hygroscopic aerosol have found large increases in nocturnal stomatal conductance (80–90 %) when stomatal aperture was at a minimum, decreasing to less than 30 % for (i) fully open stomata when water vapor dominates transpiration (Burkhardt et al., 2001b) and (ii) 7 h post exposure, presumably due to stomatal uptake of dissolved ions through thin aqueous films (Motai et al., 2018)—the latter indicating that wicking via HAS requires continuous deposition of hygroscopic material to leaf cuticles in order to maintain a sufficient osmotic gradient. Cuticle loads of hygroscopic material of up to 50 μg cm^{-2} in these exposure studies were in the range found on urban trees (Burkhardt, 2010).

Considering the evidence for a liquid phase water loss pathway via HAS on plants exposed to moderate levels of hygroscopic aerosol, overprediction of stomatal conductance may exist in studies conducted near developed environments, especially under dark conditions when stomatal aperture is at a minimum and wicking from HAS therefore a larger relative fraction of total foliar water loss. Chamber studies may be particularly susceptible to this overprediction given the mechanically mixed conditions often used to minimize diffusive boundary layer resistances (Burkhardt et al., 2001b; Pariyar et al., 2013), thereby confounding partitioning of non-stomatal and stomatal deposition pathways under dark conditions from scaled estimates of stomatal conductance to water vapor.

Surface area also plays an important role in gaseous uptake within the interior of leaves. Nobel et al. (1975) found that a 4-fold increase in CO_2 uptake between shade and sun leaves of the deciduous species 'Creeping Charlie' (*Plectranthus parviflorus*) could be explained by the corresponding increase in mesophyll cell surface area per unit projected leaf area ($A^{mes}/A^{projected}$), and that internal leaf resistance to CO_2 per unit area of mesophyll (A^{mes}) remained constant. To our knowledge, no such analysis has been conducted for foliar uptake of NO_2. Delaria et al. (2020) provide estimates of mesophilic resistance (r_m) for NO_2 to six coniferous and four deciduous tree species native to California, with values of r_m ranging from 20–130 s m^{-1} (median 48 s m^{-1}, mean 57 s m^{-1}) per unit projected leaf area, which at the forest canopy scale would represent a small (< 5 %) and modest (~ 15 %) fraction of bulk-canopy $R_c(NO_2)$ for nighttime and daytime conditions at Harvard Forest, respectively, during summer (Fig. S8 & Table S3). Nonetheless, using the $A^{mes}/A^{projected}$ value of 50 corresponding to deciduous sun leaves from Nobel et al. (1975) and the NO_2 uptake coefficient to distilled water of 2.3 x 10^{-6} (Table 1), an estimate of r_m due to uptake on moist intercellular leaf surfaces is ~ 100 s m^{-1}. This suggests, on average, an additional pathway for NO_2 uptake to leaf interiors with a resistance on the order of 100 s m^{-1} is acting in parallel to reaction R1—a likely pathway being NO_2 scavenging by apoplastic antioxidants (Farvardin et al., 2020; Msibi et al., 1993; Ramge et al., 1993; Teklemariam and Sparks, 2006). The assumption that the ratio $A^{mes}/A^{projected} \sim 50$ is representative and constant across the species examined by Delaria et al. (2020) is a generalized approximation and further work is required to understand the mechanisms driving intra- and interspecies variability in r_m. Future leaf-level study into the mechanism of foliar NO_2 uptake would benefit from consideration of possible HAS, $A^{mes}/A^{projected}$, as well as apoplastic antioxidant concentrations.

Additional supplemental figures and tables

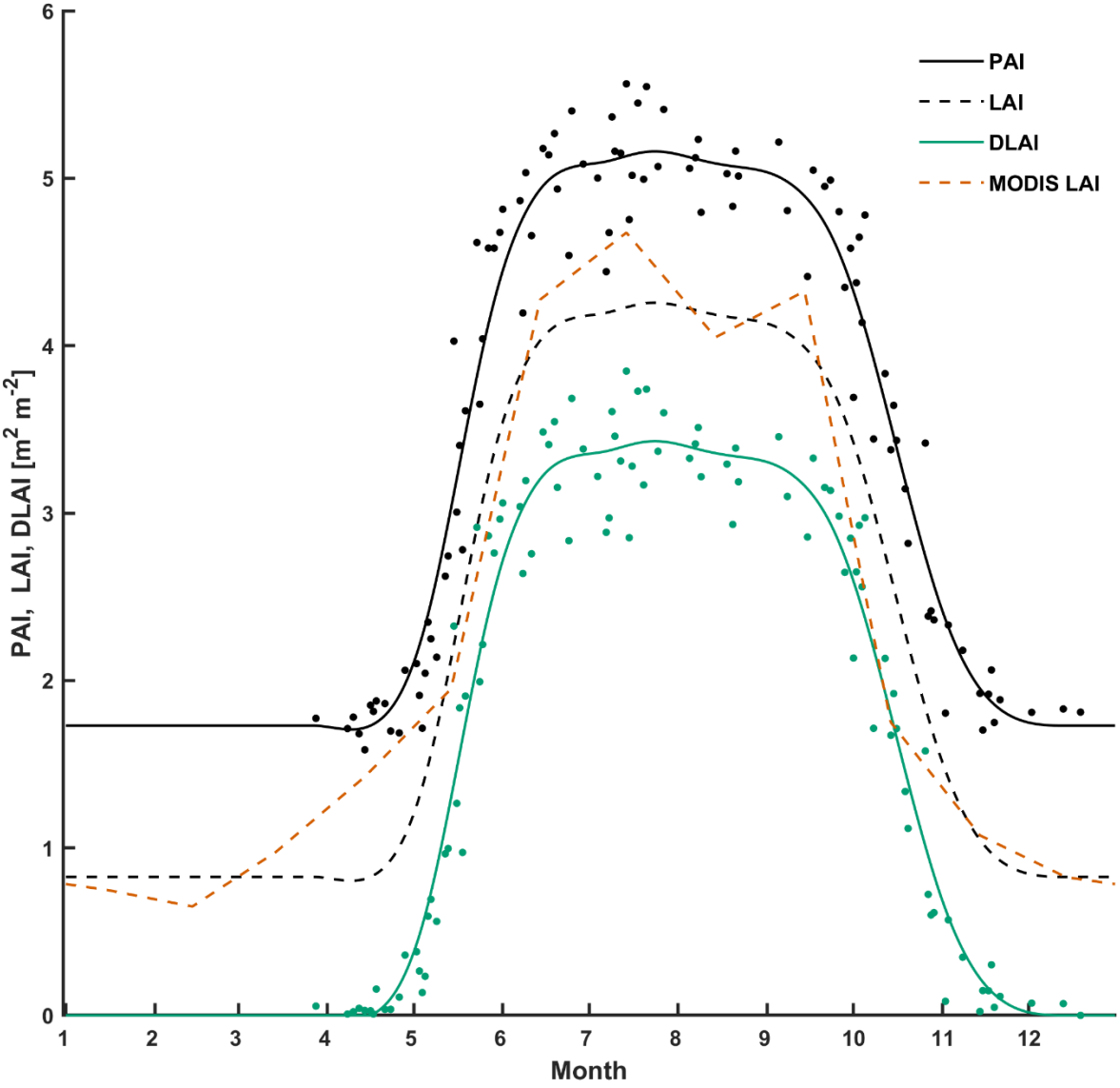

Figure S5: Observed plant area index (**PAI**) and deciduous leaf area index (**DLAI**) at Harvard Forest from 1998–2015. Leaf area index (**LAI**) includes both deciduous and coniferous foliage and is computed herein as a spline-fit to observed PAI corrected for reported stem and twig area index (STAI = 0.9). Also depicted is a multiyear mean (2005–2008) **MODIS LAI** for the corresponding 0.25˚ x 0.25˚ grid cell. Dots depict measurements of PAI and DLAI obtained from the Harvard Forest Data Archive (Matthes et al., 2024). STAI = 0.9 was reported by Horii et al. (2005).

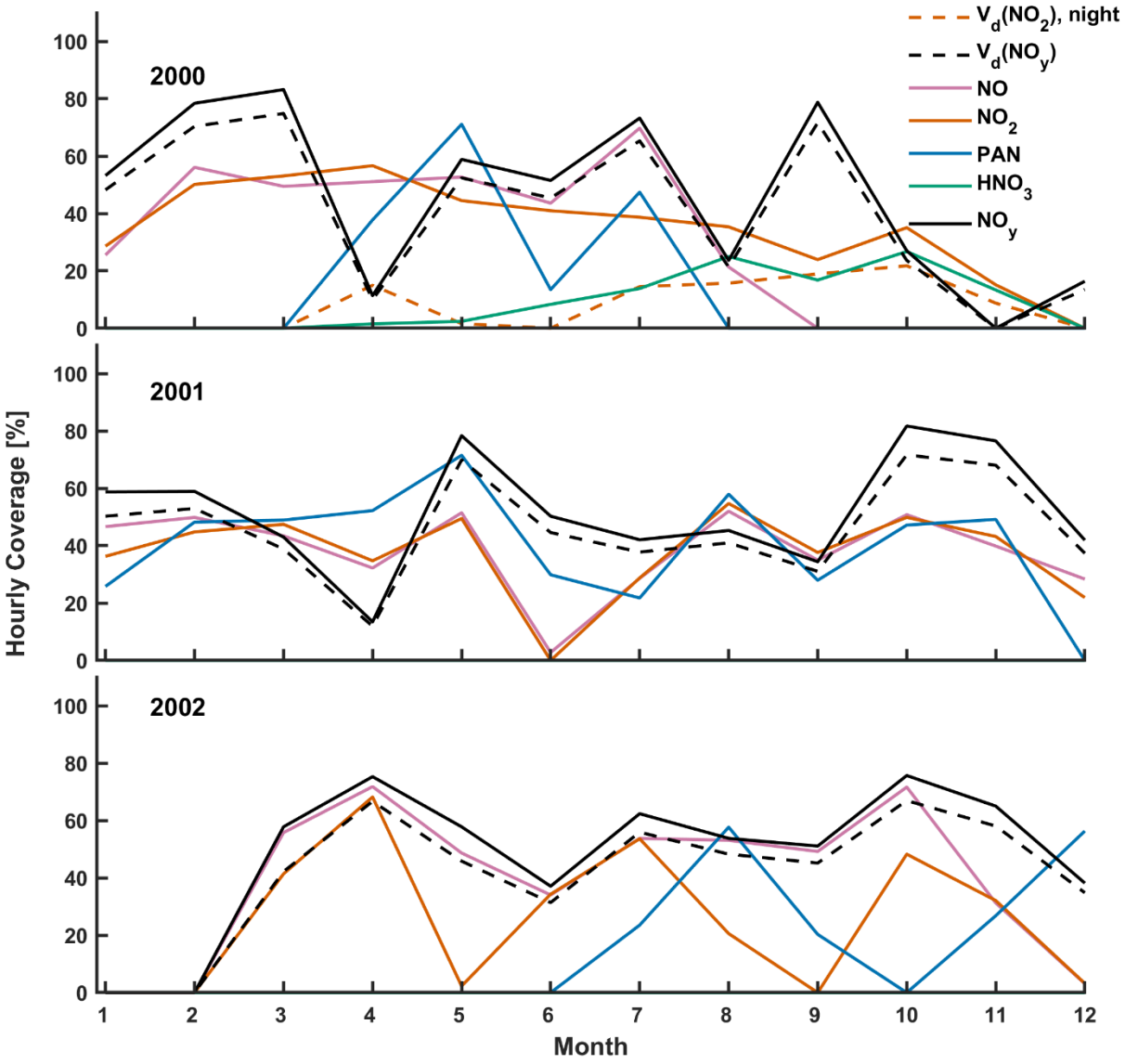

Figure S6: Hourly coverage of measured above-canopy trace gas concentrations and eddy covariance observed exchange velocities at Harvard Forest from 2000–2002. Measurements taken during conditions of low turbulence ($u_* < 0.2$ m s^{-1}) were omitted from analysis (Section 2.2.2).

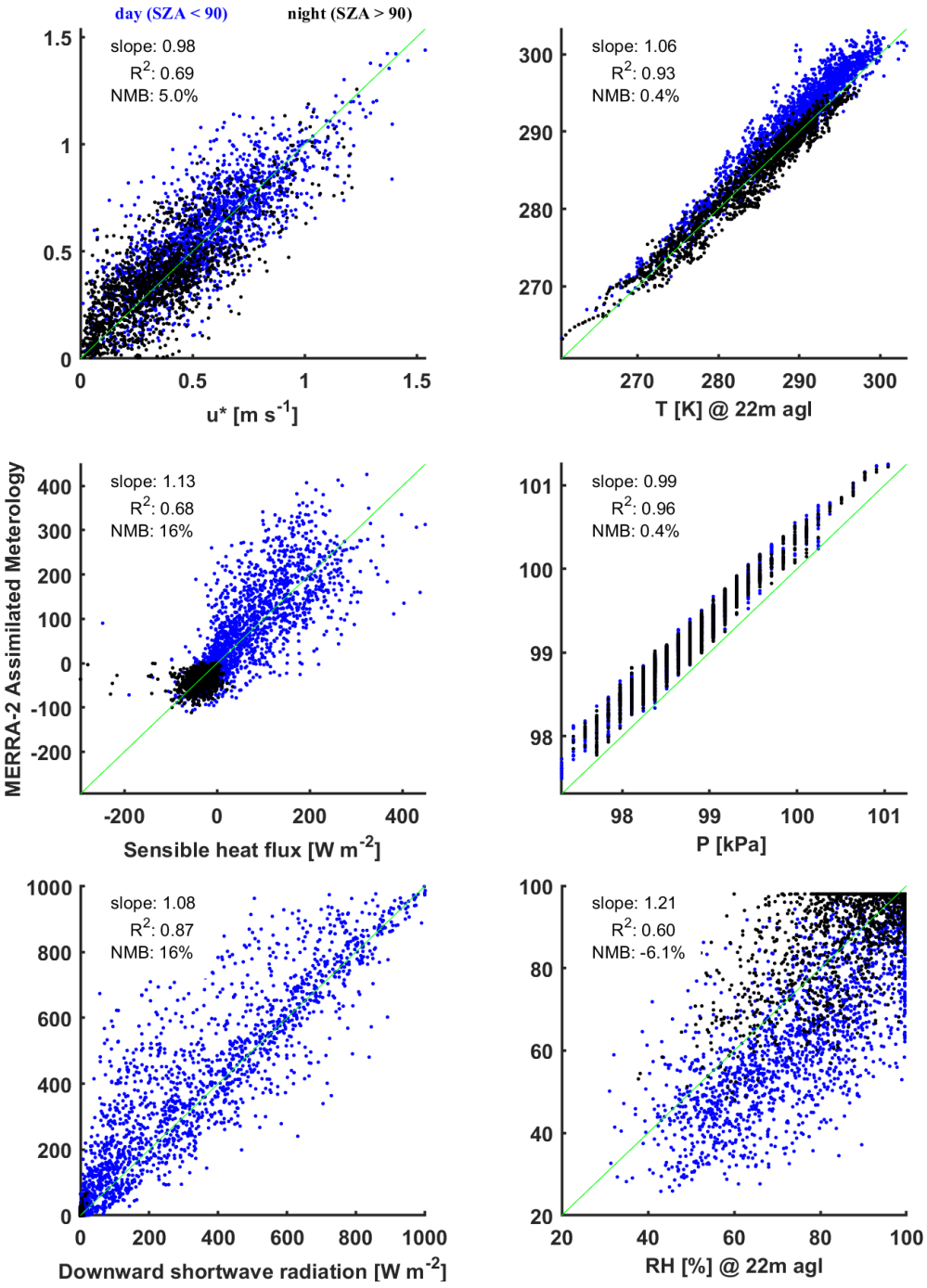

Figure S7: Comparisons of hourly observations of friction velocity u_*, sensible heat flux, downward shortwave radiation, *T*, *P*, and *RH* made over Harvard Forest to coincident values from GEOS assimilated meteorological fields (MERRA2 at 0.5˚ x 0.625˚). Daytime observations are shown for solar zenith angles SZA < 90° and nighttime for SZA > 90°. Striations in comparison of pressure result from measured values reported on 133 Pa intervals.

Table S1: Compilation of binary gas phase diffusion coefficients in air or N_2 for atmospherically relevant molecules. Computed values following the semi-empirical technique of Fuller's method are tabulated alongside measured values where available. Diffusivities (D_o) are reported at 273 K and 101325 Pa following Eq. (3)**.**

Species	**Fuller's Method**	**Measured**		**Ref.**[(a)]
	D_o ($cm^2\ s^{-1}$)	D_o ($cm^2\ s^{-1}$)		
inorganics				
HNO_3	0.130	0.099	± 0.008	1
NO_3	0.142	0.105	± 0.053	1
HONO	0.151	0.110	± 0.03	1
NH_3	0.228	0.201	± 0.011	1
SO_2	0.115	0.107	± 0.015	1
H_2SO_4	0.094	0.085	± 0.011	1
H_2O_2	0.168	0.133	± 0.04	1
HOBr	0.115	0.096	± 0.01	1
HBr	0.127	0.109	± 0.033	1
HCl	0.148	0.135	± 0.008	1
Cl_2	0.106	0.107	± 0.011	1
I_2	0.083	0.061	± 0.015	1
Br_2	0.096	0.086	± 0.007	1
NO_2	0.157	0.145	± 0.001	2
N_2O_4	0.111	0.084	± 0.004	2
N_2O_5	0.103	0.081	± 0.005	2
$ClONO_2$	0.100	0.085	± 0.001	2
O_3	0.152	0.153	± 0.001	2
H_2O	0.229	0.218		3
CO_2	0.133	0.138		3
N_2O	0.164	0.144		3
CO	0.161	0.181		3
NO	0.199	0.180		3
organics				
methane	0.181	0.190	± 0.006	4
ethane	0.122	0.129	± 0.006	4
propane	0.097	0.098	± 0.006	4
ethylene	0.129	0.140	± 0.006	4
benzene	0.077	0.081	± 0.003	4
toluene	0.069	0.076	± 0.005	4
xylene	0.064	0.061	± 0.006	4
methanol	0.138	0.142	± 0.012	4
ethanol	0.106	0.111	± 0.008	4
acetone	0.091	0.092	± 0.006	4
methyl ethyl ketone	0.082	0.078	± 0.002	4
formic acid	0.125	0.131	± 0.005	4
acetic acid	0.100	0.106	± 0.006	4
peroxyacetyl nitrate	0.080	-		-
Hydroxymethyl hydroperoxide	0.107			
CCl_4	0.070	0.069	± 0.003	5
CH_2Cl_2	0.090	0.089	± 0.005	5
$CHCl_3$	0.078	0.078	± 0.003	5
$CHBr_3$	0.073	0.066	± 0.001	5

[(a)] References for measured diffusion coeficients:
(1) Tang et al. (2014)
(2) Langenberg et al. (2020)
(3) Massman (1998)
(4) Tang et al. (2015)
(5) Gu et al. (2018)

Table S2: Inferred NO_2 uptake coefficients γ_{NO_2} to both non-foliar and foliar materials from literature values of surface deposition velocities V_d^{surf}. Abbreviations used: Eddy Covariance (EC), Coniferous (C), Deciduous (D), Broadleaf (BL), Non-Stomatal (NS), Table (T), and Figure (F).

Material	Measurement Technique	V_d^{surf}	γ_{NO_2} [a]	Surface Area [b]	T	RH	Ref. [j]
	method/location/condition	[cm s^{-1}]	[unitless]		[°C]	[%]	
Non-Foliar Surfaces							
Teflon	chamber/ lab	~ 0	~ 0	total	29.4	unknown	1
distilled water	chamber/ lab	0.021	2.3 x 10^{-6}	total (planar)	29.4	N/A	1
concreate (fine)	chamber/ lab	0	0	geometric	22	30	2, T5
		0.01	1.1 x 10^{-6}			50	
		0.01	1.1 x 10^{-6}			90	
concrete (coarse)	chamber/ lab	0	0	geometric	22	30	2, T5
		0.02	2.2 x 10^{-6}			50	
		0.03	3.3 x 10^{-6}			70	
		0.03	3.3 x 10^{-6}			90	
wood board (untreated,	chamber/ lab	0	0	geometric	22	50	2, T5
hard, fine, aged)		0.007	7.6 x 10^{-7}			70	
		0.015	1.6 x 10^{-6}			90	
plywood (untreated)	chamber/ lab	0.013	1.4 x 10^{-6}	geometric	unknown [c]	50	2, T2
tree bark (wet)	chamber/ lab	0.093	1.0 x 10^{-5}	geometric	29.4	N/A	1
tree bark (dry)	chamber/ lab	0.047	5.0 x 10^{-6}	geometric	29.4	unknown	1
forest floor (hardwood)	chamber/ lab	0.47	5.0 x 10^{-5}	planar	29.4	unknown	1
forest floor (coniferous)	chamber/ lab	0.48	5.1 x 10^{-5}	planar			1
forest floor	chamber/ field	0.40	4.3 x 10^{-5}	planar	~20 ± 6	~60 ± 20	3
snow	EC/ prairie/ winter	0.14	1.6 x 10^{-5}	planar	-20 to 0	N/A	4 [d]
Foliar Surfaces							
White pine (Pinus strobus): C	chamber/field/ NS at g_{H_2O}= 0	0.043	4.7 x 10^{-6}	projected leaf area	~20	ambient	5 [f]
		0.016	1.7 x 10^{-6}	total leaf area [e]			
10 tree species: 6 C, 2 D, 2 BL	chamber/ lab/dark				20	<90	6 [g]
-average of 6 C species		0.034 (0.009–0.087)	3.7 x 10^{-6}	projected leaf area			6, T2 [h]
		0.013	1.4 x 10^{-6}	total leaf area [e]			
-average of 2 D & 2 BL species		0.017 (0.004–0.037)	1.9 x 10^{-6}	projected leaf area			6, T2 [h]
CA Oak (Quercus agrifolia): BL	chamber/ lab/ dark	0.015	1.6 x 10^{-6}	projected leaf area	22	50–65	7, T1

5 tree species: 3 D, 1 BL, 1 C	chamber/ lab/						8[g]
-average of all 5 species (~ D & BL)	dark	0.012 (0.004–0.021)	1.3 x 10^{-6}	projected leaf area	20 ± 3	50 ± 4	8, F7[h]
2 tree species: 2 C (avg. of 2 C	chamber/ field/ dark	0.056 (0.03–0.08)	6.2 x 10^{-6}	projected leaf area	~10–14	~50–70	3[g], T2[h]
species Norway Spruce & Scots Pine)		0.021	2.3 x 10^{-6}	total leaf area[e]			
8 tree species: 3 C, 5 D	chamber/ lab/				29.4	unknown	1
-average of 3 C species	dark (min g_{H_2O})	0.015 (-0.003–0.03)	1.6 x 10^{-6}	total leaf area			1, F4[h,i]
		0.041	4.3 x 10^{-6}	projected leaf area			
-average of 5 D species	NS at g_{H_2O}= 0	0.014	1.5 x 10^{-6}	projected leaf area			1, T2[i]
Norway Spruce (Picea abies L.): C	chamber/ field/ dark	0.014	1.5 x 10^{-6}	projected leaf area	~12 ± 3	~82 ± 12	9[g], T2[i]
		0.0052	5.7 x 10^{-7}	total leaf area[e]			
	Deciduous/Broadleaf (average)	**0.015**	**1.6 x 10^{-6}**	**projected leaf area**		**50 to <90**	**1,6-8**
	Coniferous (average)	**0.038**	**4.1 x 10^{-6}**	**projected leaf area**		**50 to <90**	**1,3,5,6,9**
	Coniferous (average)	**0.014**	**1.5 x 10^{-6}**	**total leaf area[e]**		**50 to <90**	**1,3,5,6,9**

[a] Uptake coefficients for NO_2 inferred herein from literature values of surface deposition velocities: $\gamma_{NO_2} = 4\, v_d^{surf}\, \bar{v}_t^{-1}$, where $\bar{v}_t$ is the mean thermal speed of NO_2, and v_d^{surf} the surface-specific deposition velocity measured from well-mixed (minimal $R_a + R_b$) chamber studies, with the exception of uptake to snow which was measured via the eddy covariance technique.

[b] Surface area used to normalize surface-specific deposition fluxes in the computation of surface-specific v_d^{surf}.

[c] Assume chamber temperature of 20 °C for calculating γ_{NO_2}.

[d] v_d^{surf} to snow was computed herein from reported eddy covariance (EC) inferred $R_c(NO_2)$ to snow of 740 ± 210 s m^{-1}; we compute $\bar{v}_t$ at 260 K.

[e] Reported v_d^{surf} for coniferous species normalized to projected leaf area is scaled herein to reflect uptake to total leaf surface area—a factor of 2.7 for coniferous needles (see Section 2.4).

[f] 3 D species reported with NS v_d^{surf} (at g_{H_2O}= 0) not significantly different from zero, which we omit from analysis due to inability to compute v_d^{surf} for dark conditions.

[g] References which find stomatal conductance sufficient to explain observed NO_2 uptake.

[h] Mean value averaged herein from values reported in indicated table or estimated from indicated figure (i.e., T2 = Table 2; F7 = Fig. 7) of reference.

[i] v_d^{surf} computed herein by normalizing reported (from Table) or estimated (from Figure) mean NO_2 flux by mean concentration.

[j] References for surface-specific $v_d^{surf}(NO_2)$

(1) Hanson et al. (1989)
(2) Grøntoft and Raychaudhuri (2004)
(3) Rondón et al. (1993)
(4) Stocker et al. (1995)
(5) Wang et al. (2020)
(6) Delaria et al. (2020)
(7) Delaria et al. (2018)
(8) Chaparro-Suarez et al. (2011)
(9) Breuninger et al. (2013)

Table S3: Monthly mean nocturnal (20:00–04:00 LST) above-canopy $V_d(NO_2)$ at Harvard Forest computed using bulk-canopy $R_c(NO_2)$ parameterized following: (i) Z03 scheme; (ii) bottom-up estimates of component canopy surface resistances using surface-specific NO_2 uptake coefficients (Table 1) and relevant surface area scaling; (iii) r_{hyd} following Eq. (8) with top-down constraints on the surface area scaling term α.

	Jan.	Feb.	March	April	May	June	July	Aug.	Sept.	Oct.	Nov.	Dec.
Canopy Conditions [a]												
T @ 15 m [°C]	-7.0	-6.7	-0.3	3.9	9.2	15	17	19	14	7.2	2.4	-2.7
RH @ 15 m [%]	83	72	83	72	86	93	92	92	95	90	87	79
LAI	0.83	0.83	0.83	0.83	2.2	4.1	4.2	4.2	4.0	2.6	1.0	0.83
u_* [m s^{-1}]	0.52	0.58	0.53	0.45	0.43	0.39	0.36	0.36	0.39	0.40	0.51	0.55
Aerodynamic Res. [b]												
R_a(29 m) [s m^{-1}]	11.6	10.1	11.3	13.9	13.2	14.9	16.9	17.3	15.7	14.6	10.7	12.0
Quasi-Laminar Res. [b]												
R_b(NO2) [s m^{-1}]	14.0	12.1	12.8	14.9	14.8	16.4	17.8	16.7	16.3	15.4	12.6	12.5
Z03 $V_d(NO_2)$ [c]												
R_c, canopy [s m^{-1}]	691	652	574	645	673	676	715	788	600	652	527	638
V_d [cm s^{-1}]	0.17	0.21	0.23	0.19	0.19	0.18	0.16	0.20	0.20	0.20	0.24	0.20
Bottom-up $V_d(NO_2)$ [d]												
r_c, leaf [s m^{-1}]	3410	3410	3370	3250	1850	1070	1010	1060	1140	1720	2990	3380
r_c, bark [s m^{-1}]	779	782	725	707	637	578	579	617	624	666	682	736
r_a, canopy [s m^{-1}]	573	495	561	691	1350	2480	3040	3040	2480	1590	628	513
r_c, floor [s m^{-1}]	307	296	284	272	260	256	255	254	256	263	273	291
R_c, canopy [s m^{-1}]	352	324	313	347	324	305	315	327	329	345	303	315
R_c, canopy [s m^{-1}] [e]	464	419	411	469	444	422	435	450	451	473	401	412
V_d [cm s^{-1}]	0.28	0.31	0.32	0.29	0.30	0.32	0.30	0.30	0.30	0.29	0.33	0.32
V_d [cm s^{-1}] [e]	0.22	0.25	0.25	0.22	0.23	0.23	0.23	0.22	0.22	0.22	0.26	0.25
Top-down $V_d(NO_2)$ [f]												
$R_c = r_{hyd}$(α=1) [s m^{-1}]	881	1013	928	1087	969	822	795	728	774	896	847	924
$R_c = r_{hyd}$(α=2) [s m^{-1}]	456	531	474	549	485	411	397	364	387	450	427	475
V_d (α=1) [cm s^{-1}]	0.11	0.1	0.11	0.1	0.11	0.12	0.12	0.13	0.13	0.11	0.12	0.11
V_d (α=2) [cm s^{-1}]	0.21	0.19	0.21	0.19	0.21	0.24	0.24	0.26	0.24	0.22	0.23	0.21

[a] T, RH, and u_* are nocturnal (2000–0400 LST) monthly medians from an hourly data set spanning 2000–2002. Periods of low turbulence ($u_* < 0.2$ m s^{-1}) were excluded from analysis.
[b] Above-canopy aerodynamic resistance computed as $R_a(29m) = u\ (29\ m)/u_*^2$; quasi-laminar boundary layer resistance R_b computed following Eq. (S2).
[c] Nocturnal $V_d(NO_2)$ following the Z03 scheme (Zhang et al., 2003), as described in Section 2.1.2.
[d] Bottom-up $V_d(NO_2)$ computed following Eq. (2), with $R_c(NO_2)$ following Eq. (10). Component $r_c = 4/(\bar{v}_t\ \gamma\ \alpha)$, where uptake coefficients are from Table 1, as described in Section 3.3.4.
[e] Computed with uptake to bark reduced by a factor of two (i.e., 2 x r_c bark) (Section 3.3.4).
[f] Top-down $V_d(NO_2)$ computed following Eq. (2) and r_{hyd} following Eqs. (8–9). Snow fraction is computed following Z03, and $\bar{\gamma}_{snow}$ = 1.6 x 10^{-5} is used for all available surface area for r_{hyd}, α = 1, and ½ of available surface area for r_{hyd}, α = 2.

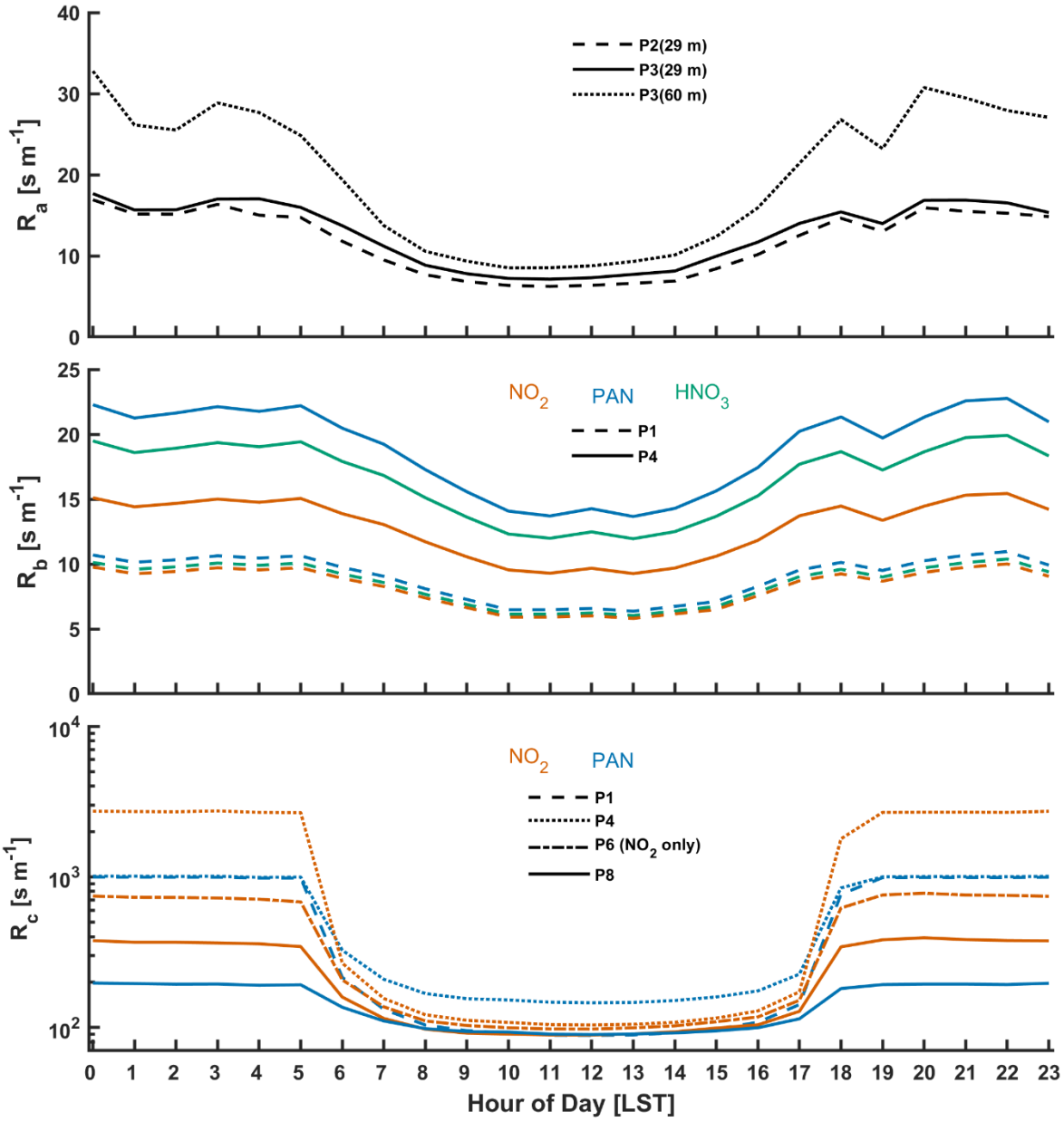

Figure S8: Median component resistances R_a, R_b, and R_c from parameterized deposition velocities for HNO_3, NO_2, and PAN over Harvard Forest. Aerodynamic resistance R_a is common to all species and depicted for parameterizations P2 and P3 computed from the 29 m or 60 m measurement height, as indicated. Quasi-laminar boundary layer resistance R_b is shown for all species according to parameterizations P1 and P4. Surface layer resistances R_c for NO_2 and PAN are depicted for parameterizations P1, P4, P6, and P8 (equivalent to P7 for NO_2; Table 2).

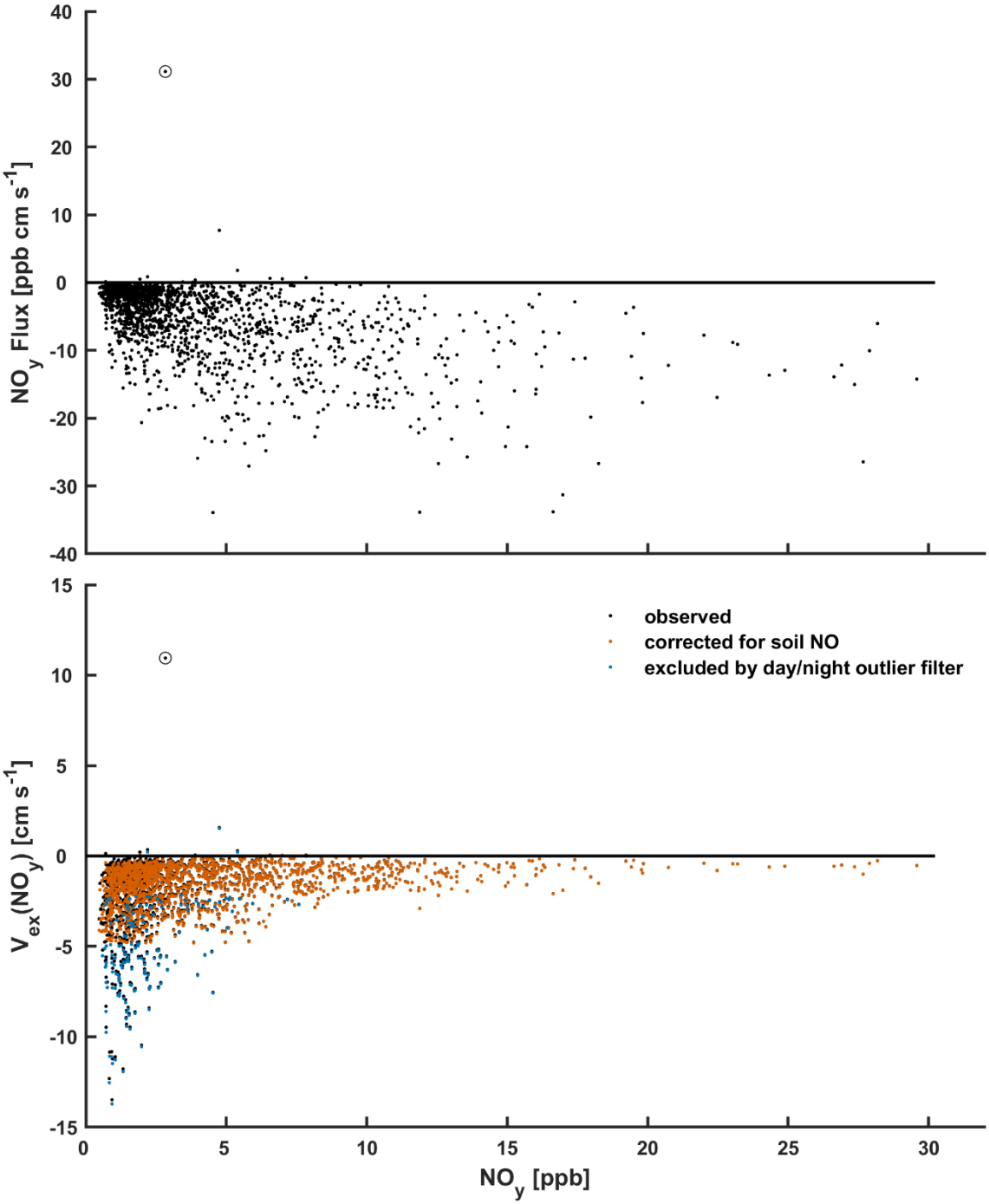

Figure S9: (TOP) Hourly eddy covariance NO_y fluxes and **(BOTTOM)** resulting exchange velocities $V_{ex(NO_y)}$ as a function of NO_y concentration over Harvard Forest. These publicly available measurements (Section 2.2.2) were made over an established mixed deciduous forest (Harvard Forest, MA, U.S.) from June–November 2000. Estimated above-canopy soil NO flux was subtracted from measured hourly NO_y fluxes in order to estimate $V_{ex(NO_y)}$ due to deposition (depicted as 'corrected for soil NO'). Data excluded by a day/night $V_{ex(NO_y)}$ outlier filter are shown in blue. Data points excluded from analysis based on visual inspection are circled. Hourly observations made under conditions of low turbulence ($u_* < 0.2$ m s^{-1}) were excluded from analysis (Section 2.2.2).

References

Ammann, M., Rössler, E., Strekowskit, R. and George, C.: Nitrogen dioxide multiphase chemistry: Uptake kinetics on aqueous solutions containing phenolic compounds, Phys. Chem. Chem. Phys., 7(12), 2513–2518, doi:10.1039/b501808k, 2005.

Ammann, M., Cox, R. A., Crowley, J. N., Jenkin, M. E., Mellouki, A., Rossi, M. J., Troe, J. and Wallington, T. J.: Evaluated kinetic and photochemical data for atmospheric chemistry: Volume VI - Heterogeneous reactions with liquid substrates, Atmos. Chem. Phys., 13(16), 8045–8228, doi:10.5194/acp-13-8045-2013, 2013.

Arnqvist, J. and Bergström, H.: Flux-profile relation with roughness sublayer correction, Q. J. R. Meteorol. Soc., 141(689), 1191–1197, doi:10.1002/qj.2426, 2015.

Bambauer, A., Brantner, B., Paige, M. and Novakov, T.: Laboratory Study of NO2 Reaction With Dispersed and Bulk Liquid Water, Atmos. Environ., 28(20), 3225–3232, 1994.

Bang, J., Lee, D. H., Kim, S.-K. and Kang, H.: Reaction of nitrogen dioxide with ice surface at low temperature (≤170 K), J. Phys. Chem. C, 119(38), 22016–22024, doi:10.1021/acs.jpcc.5b05497, 2015.

Bannister, E. J., Jesson, M., Harper, N. J., Hart, K. M., Curioni, G., Cai, X. and MacKenzie, A. R.: Residence times of air in a mature forest: observational evidence from a free-air CO2 enrichment experiment, Atmos. Chem. Phys., 23(3), 2145–2165, doi:10.5194/acp-23-2145-2023, 2023.

Breuninger, C., Meixner, F. X. and Kesselmeier, J.: Field investigations of nitrogen dioxide (NO2) exchange between plants and the atmosphere, Atmos. Chem. Phys., 13(2), 773–790, doi:10.5194/acp-13-773-2013, 2013.

Bröske, R., Kleffmann, J. and Wiesen, P.: Heterogeneous conversion of NO2 on secondary organic aerosol surfaces: a possible source of nitrous acid (HONO) in the atmosphere?, Atmos. Chem. Phys., 3(3), 469–474, doi:10.5194/acp-3-469-2003, 2003.

Bryan, A. M., Bertman, S. B., Carroll, M. A., Dusanter, S., Edwards, G. D., Forkel, R., Griffith, S., Guenther, A. B., Hansen, R. F., Helmig, D., Jobson, B. T., Keutsch, F. N., Lefer, B. L., Pressley, S. N., Shepson, P. B., Stevens, P. S. and Steiner, A. L.: In-canopy gas-phase chemistry during CABINEX 2009: Sensitivity of a 1-D canopy model to vertical mixing and isoprene chemistry, Atmos. Chem. Phys., 12(18), 8829–8849, doi:10.5194/acp-12-8829-2012, 2012.

Burkhardt, J.: Hygroscopic particles on leaves: nutrients or desiccants?, Ecol. Monogr., 80(3), 369–399, doi:10.1890/09-1988.1, 2010.

Burkhardt, J. and Eiden, R.: Thin water films on coniferous needles, Atmos. Environ., 28(12), 2001–2017, doi:10.1016/1352-2310(94)90469-3, 1994.

Burkhardt, J. and Hunsche, M.: " Breath figures " on leaf surfaces — formation and effects of microscopic leaf wetness, Front. Plant Sci., 4, Article 422, doi:10.3389/fpls.2013.00422, 2013.

Burkhardt, J., Kaiser, H., Goldbach, H. and Kappen, L.: Measurements of electrical leaf surface conductance reveal recondensation of transpired water vapour on leaf surfaces, Plant, Cell Environ., 22(2), 189–196, doi:10.1046/j.1365-3040.1999.00387.x, 1999.

Burkhardt, J., Koch, K. and Kaiser, H.: Deliquescence of Deposited Atmospheric Particles on Leaf Surfaces, Water, Air, Soil Pollut. Focus, 1, 313–321, doi:10.1023/A:1013179810839, 2001a.

Burkhardt, J., Kaiser, H., Kappen, L. and Goldbach, H. E.: The possible role of aerosols on stomatal conductivity for water vapour, Basic Appl. Ecol., 2(4), 351–364, doi:10.1078/1439-1791-00062, 2001b.

Burkhardt, J., Zinsmeister, D., Grantz, D. A., Vidic, S., Sutton, M. A., Hunsche, M. and Pariyar, S.: Camouflaged as degraded wax: hygroscopic aerosols contribute to leaf desiccation , tree mortality , and forest decline, Environ. Res. Lett., 13, 085001, doi:10.1088/1748-9326/aad346, 2018.

Cellier, P. and Brunet, Y.: Flux-gradient relationships above tall plant canopies, Agric. For. Meteorol., 58, 93–117, doi:10.1016/0168-1923(92)90113-I, 1992.

Chaparro-Suarez, I. G., Meixner, F. X. and Kesselmeier, J.: Nitrogen dioxide (NO2) uptake by vegetation controlled by atmospheric concentrations and plant stomatal aperture, Atmos. Environ., 45(32), 5742–5750, doi:10.1016/j.atmosenv.2011.07.021, 2011.

Cheung, J. L., Li, Y. Q., Boniface, J., Shi, Q., Davidovits, P., Worsnop, D. R., Jayne, J. T. and Kolb, C. E.: Heterogeneous Interactions of NO2 with Aqueous Surfaces, J. Phys. Chem. A, 104(12), 2655–2662, doi:10.1021/jp992929f, 2000.

Clifton, O. E., Fiore, A. M., Munger, J. W., Malyshev, S., Horowitz, L. W., Shevliakova, E., Paulot, F., Murray, L. T. and Griffin, K. L.: Interannual variability in ozone removal by a temperate deciduous forest, Geophys. Res. Lett., 44(1), 542–552, doi:10.1002/2016GL070923, 2017.

Collins, D. B., Hems, R. F., Zhou, S., Wang, C., Grignon, E., Alavy, M., Siegel, A. and Abbatt, J. P. D.: Evidence for gas−surface equilibrium control of indoor nitrous acid, Environ. Sci. Technol., 52, 12419–12427, doi:10.1021/acs.est.8b04512, 2018.

Colussi, A. J. and Enami, S.: Detecting intermediates and products of fast heterogeneous reactions on liquid surfaces via online mass spectrometry, Atmosphere (Basel)., 10(47), doi:10.3390/atmos10020047, 2019.

Costa, J. M., Monnet, F., Jannaud, D., Leonhardt, N., Ksas, B., Reiter, I. M., Pantin, F. and Genty, B.: Open all night long: the dark side of stomatal control, Plant Physiol., 167, 289–294, doi:10.1104/pp.114.253369, 2015.

Delaria, E. R. and Cohen, R. C.: A model-based analysis of foliar NOx deposition, Atmos. Chem. Phys., 20, 2123–2141, doi:10.5194/acp-20-2123-2020, 2020.

Delaria, E. R., Vieira, M., Cremieux, J. and Cohen, R. C.: Measurements of NO and NO2 exchange between the atmosphere and Quercus agrifolia, Atmos. Chem. Phys., 18, 14161–14173, doi:10.5194/acp-18-14161-2018, 2018.

Delaria, E. R., Place, B. K., Liu, A. X. and Cohen, R. C.: Laboratory measurements of stomatal NO2 deposition to native California trees and the role of forests in the NOx cycle, Atmos. Chem. Phys., 20, 14023–14041, doi:10.5194/acp-2020-240, 2020.

Dyer, A. J.: A Review of Flux-Profile Relationships, Boundary-Layer Meteorol., 7, 363–372, doi:10.1007/BF00240838, 1974.

Eugster, W. and Hesterberg, R.: Transfer resistances of NO2 determined from eddy correlation flux measurements over a litter meadow at a rural site on the Swiss plateau, Atmos. Environ., 30(8), 1247–1254, doi:10.1016/1352-2310(95)00418-1, 1996.

Farvardin, A., Isabel, A., Llorens, E., Garc, P., Scalschi, L. and Vicedo, B.: The Apoplast: A Key Player in Plant Survival, Antioxidants, 9(604), doi:10.3390/antiox9070604, 2020.

Finlayson-Pitts, B. J.: Reactions at surfaces in the atmosphere: integration of experiments and theory as necessary (but not necessarily sufficient) for predicting the physical chemistry of aerosols, Phys. Chem. Chem. Phys., 11(36), 7760–7779, doi:10.1039/B906540G, 2009.

Finlayson-Pitts, B. J., Wingen, L. M., Sumner, A. L., Syomin, D. and Ramazan, K. A.: The heterogeneous hydrolysis of NO2 in laboratory systems and in outdoor and indoor atmospheres: An integrated mechanism, Phys. Chem. Chem. Phys., 5(2), 223–242, doi:10.1039/B208564J, 2003.

Finnigan, J.: Turbulence in plant canopies, Annu. Rev. Fluid Mech., 35, 519–571, doi:10.1146/annurev.fluid.32.1.519, 2000.

Finnigan, J. J., Shaw, R. H. and Patton, E. G.: Turbulence structure above a vegetation canopy, J. Fluid Mech., 637, 387–424, doi:10.1017/S0022112009990589, 2009.

Gallo, A., Farinha, A. S. F., Emwas, A. H., Santana, A., Nielsen, R. J., Goddard, W. A. and Mishra, H.: Reply to the 'Comment on "The chemical reactions in electrosprays of water do not always correspond to those at the pristine air–water interface"' by A. J. Colussi and S. Enami, Chem. Sci., 2019, 10, DOI: 10.1039/c9sc00991d, Chem. Sci., 10, 8256–8261, doi:10.1039/c9sc02702e, 2019a.

Gallo, A., Farinha, A. S. F., Dinis, M., Emwas, A. H., Santana, A., Nielsen, R. J., Goddard, W. A. and Mishra, H.: The chemical reactions in electrosprays of water do not always correspond to those at the pristine air-water interface, Chem. Sci., 10(9), 2566–2577, doi:10.1039/c8sc05538f, 2019b.

Garratt, J. R.: Surface influence upon vertical profiles in the atmospheric near-surface layer, Q. J. R. Meteorol. Soc., 106, 803–819, doi:10.1002/qj.49710645011, 1980.

Garratt, J. R.: The atmospheric boundary layer, Cambridge University Press., 1992.

Gerken, T., Chamecki, M. and Fuentes, J. D.: Air-Parcel Residence Times Within Forest Canopies, Boundary-Layer Meteorol., 165, 29–54, doi:10.1007/s10546-017-0269-7, 2017.

Grantz, D. A., Zinsmeister, D. and Burkhardt, J.: Ambient aerosol increases minimum leaf conductance and alters the aperture–flux relationship as stomata respond to vapor pressure deficit (VPD), New Phytol., 219, 275–286, doi:10.1111/nph.15102, 2018.

Grøntoft, T. and Raychaudhuri, M. R.: Compilation of tables of surface deposition velocities for O3, NO2 and SO2 to a range of indoor surfaces, Atmos. Environ., 38(4), 533–544, doi:10.1016/j.atmosenv.2003.10.010, 2004.

Gu, W., Cheng, P. and Tang, M.: Compilation and evaluation of gas phase diffusion coefficients of halogenated organic compounds, R. Soc. Open Sci., 5(7), doi:10.1098/rsos.171936, 2018.

Haghighi, E. and Or, D.: Linking evaporative fluxes from bare soil across surface viscous sublayer with the Monin-Obukhov atmospheric flux-profile estimates, J. Hydrol., 525, 684–693, doi:10.1016/j.jhydrol.2015.04.019, 2015.

Hanson, P. J. and Linderg, S. E.: Dry deposition of reactive nitrogen compounds: a review of leaf, canopy and non-foliar measurements, Atmos. Environ., 25A(8), 1615–1634, doi:10.1016/0960-1686(91)90020-8, 1991.

Hanson, P. J., Rott, K., Taylor, G. E., Gunderson, C. A., Lindberg, S. E. and Ross-Todd, B. M.: NO2 deposition to elements representative of a forest landscape, Atmos. Environ., 23(8), 1783–1794, doi:10.1016/0004-6981(89)90061-9, 1989.

Hardacre, C., Wild, O. and Emberson, L.: An evaluation of ozone dry deposition in global scale chemistry climate models, Atmos. Chem. Phys., 15(11), 6419–6436, doi:10.5194/acp-15-6419-2015, 2015.

Harman, I. N. and Finnigan, J. J.: A simple unified theory for flow in the canopy and roughness sublayer, Boundary-Layer Meteorol., 123(2), 339–363, doi:10.1007/s10546-006-9145-6, 2007.

Holtslag, A. A. M. and Bruin, H. A. R.: Applied Modeling of the Nighttime Surface Energy Balance over Land, J. Appl. Meteorol., 27, 689–703, 1988.

Holtslag, A. A. M., De Bruijn, E. I. F. and Pan, H. L.: A High Resolution Air Mass Transformation Model for Short-Range Weather Forecasting, Mon. Weather Rev., 118, 1561–1575, 1990.

Horii, C. V., Munger, J. W., Wofsy, S. C., Zahniser, M., Nelson, D. and McManus, J. B.: Fluxes of nitrogen oxides over a temperate deciduous forest, J. Geophys. Res., 109, D08305, doi:10.1029/2003JD004326, 2004.

Horii, C. V., Munger, J. W., Wofsy, S. C., Zahniser, M., Nelson, D. and Mcmanus, J. B.: Atmospheric reactive nitrogen concentration and flux budgets at a Northeastern U.S. forest site, Agric. For. Meteorol., 133, 210–225, doi:10.1016/j.agrformet.2004.08.009, 2005.

Hudman, R. C., Moore, N. E., Mebust, A. K., Martin, R. V., Russell, A. R., Valin, L. C. and Cohen, R. C.: Steps towards a mechanistic model of global soil nitric oxide emissions: Implementation and space based-constraints, Atmos. Chem. Phys., 12(16), 7779–7795, doi:10.5194/acp-12-7779-2012, 2012.

Jacob, D. J. and Wofsy, S. C.: Budgets of reactive nitrogen, hydrocarbons, and ozone over the Amazon forest during the wet season, J. Geophys. Res., 95(D10), 16737–16754, doi:10.1029/jd095id10p16737, 1990.

Kaimal, J. C. and Finnigan, J. .: Atmospheric Boundary Layer Flows: Their Structure and Measurement, Oxford University Press., 1994.

Karamchandani, P., Emery, C., Yarwood, G., Lefer, B., Stutz, J., Couzo, E. and Vizuete, W.: Implementation and refinement of a surface model for heterogeneous HONO formation in a 3-D chemical transport model, Atmos. Environ., 112, 356–368, doi:10.1016/j.atmosenv.2015.01.046, 2015.

Kinugawa, T., Enami, S., Yabushita, A., Kawasaki, M., Hoffmann, M. R. and Colussi, A. J.: Conversion of gaseous nitrogen dioxide to nitrate and nitrite on aqueous surfactants, Phys. Chem. Chem. Phys., 13(11), 5144–5149, doi:10.1039/c0cp01497d, 2011.

Kleffmann, J., Becker, K. H. and Wiesen, P.: Investigation of the heterogeneous NO2 conversion on perchloric acid surfaces, J. Chem. Soc. Faraday Trans., 94(21), 3289–3292, doi:10.1039/a805440a, 1998.

Kurtenbach, R., Becker, K. H., Gomes, J. A. G., Kleffmann, J., Lörzer, J. C., Spittler, M., Wiesen, P., Ackermann, R., Geyer, A. and Platt, U.: Investigations of emissions and heterogeneous formation of HONO in a road traffic tunnel, Atmos. Environ., 35(20), 3385–3394, doi:10.1016/S1352-2310(01)00138-8, 2001.

Lamaud, E., Loubet, B., Irvine, M., Stella, P., Personne, E. and Cellier, P.: Partitioning of ozone deposition over a developed maize crop between stomatal and non-stomatal uptakes, using eddy-covariance flux measurements and modelling, Agric. For. Meteorol., 149(9), 1385–1396, doi:10.1016/j.agrformet.2009.03.017, 2009.

Langenberg, S., Carstens, T., Hupperich, D., Schweighoefer, S. and Schurath, U.: Technical note: Determination of binary gas-phase diffusion coefficients of unstable and adsorbing atmospheric trace gases at low temperature - arrested flow and twin tube method, Atmos. Chem. Phys., 20(6), 3669–3682, doi:10.5194/acp-20-3669-2020, 2020.

Lee, Y. N. and Schwartz, S. E.: Reaction kinetics of nitrogen dioxide with liquid water at low partial pressure, J. Phys. Chem., 85(7), 840–848, doi:10.1021/j150607a022, 1981.

Lerdau, M. T., Munger, J. W. and Jacob, D. J.: The NO2 flux conundrum, Science (80-.)., 289(5488), 2291–2293, doi:10.1126/science.289.5488.2291, 2000.

Martens, C., Shay, T. J., Mendlovitz, H. P., Matross, D. M., Saleska, S. R., Wofsy, S. C., Woodward, S., Menton, M. C., De Moura, Jose, M. S., Crill, P., De Moraes, O. L. L. and Lima, R. L.: Radon fluxes in tropical forest ecosystems of Brazilian Amazonia: night-time CO2 net ecosystem exchange derived from radon and eddy covariance methods, Glob. Chang. Biol., 10, 618–629, doi:10.1111/j.1529-8817.2003.00764.x, 2004.

Massman, W. J.: A review of the molecular diffusivities of H2O, CO2, CH4, CO, O3, SO2, NH3, N2O, NO, and NO2 in air, O2 and N2 near STP, Atmos. Environ., 32(6), 1111–1127, doi:10.1016/S1352-2310(97)00391-9, 1998.

Massman, W. J., Pederson, J., Delany, A., Grantz, D., den Hartog, G., Neumann, H. H., Oncley, S. P., Pearson, R. and Shaw, R. H.: An evaluation of the regional acid deposition model surface module for ozone uptake at three sites in the San Joaquin Valley of California, J. Geophys. Res., 99(D4), 8281–8294, doi:10.1029/93JD03267, 1994.

Matthes, J., Munger, W. and Wofsy, S.: Biomass Inventories at Harvard Forest EMS Tower since 1993, Harvard Forest Data Archive: HF069 [data set], https://doi.org/10.6073/pasta/0292c5bdb53f80dffee596295cb080ca, 2024.

Mertes, S. and Wahner, A.: Uptake of nitrogen dioxide and nitrous acid on aqueous surfaces, J. Phys. Chem., 99(38), 14000–14006, doi:10.1021/j100038a035, 1995.

Min, K. E., Pusede, S. E., Browne, E. C., LaFranchi, B. W. and Cohen, R. C.: Eddy covariance fluxes and vertical concentration gradient measurements of NO and NO2 over a ponderosa pine ecosystem: observational evidence for within-canopy chemical removal of NOx, Atmos. Chem. Phys., 14, 5495–5512, doi:10.5194/acp-14-5495-2014, 2014.

Mölder, M., Grelle, A., Lindroth, A. and Halldin, S.: Flux-profile relationships over a boreal forest - Roughness sublayer corrections, Agric. For. Meteorol., 98–99, 645–658, doi:10.1016/S0168-1923(99)00131-8, 1999.

Monin, A. S. and Obukhov, A. M.: Basic laws of turbulent mixing in the surface layer of the atmosphere (Translated from Russian), Tr. Akad. Nauk SSSR Geophiz. Inst., 24(151), 163–187, 1954.

Motai, A., Yamazaki, M., Muramatsu, N., Watanabe, M. and Izuta, T.: Submicron ammonium sulfate particles deposited on leaf surfaces of a leafy vegetable (Komatsuna , Brassica rapa L . var . perviridis) are taken up by leaf and enhance nocturnal leaf conductance, Atmos. Environ., 187(May), 155–162, doi:10.1016/j.atmosenv.2018.05.064, 2018.

Msibi, I. M., Shi, J. P. and Harrison, R. M.: Accommodation coefficient for trace gas uptake using deposition profile measurement in an annular reactor, J. Atmos. Chem., 17(4), 339–351, doi:10.1007/BF00696853, 1993.

Munger, J. W., Wofsy, S. C., Bakwin, P. S., Fan, S., Goulden, M. L., Daube, B. C., Goldstein, A. H., Moore, K. E. and Fitzjarrald, D. R.: Atmospheric deposition of reactive nitrogen oxides and ozone in a temperate deciduous forest and a subarctic woodland 1. Measurements and mechanisms, J. Geophys. Res., 101, 12639–12657, doi:10.1029/96JD00230, 1996.

Murdachaew, G., Varner, M. E., Phillips, L. F., Finlayson-Pitts, B. J. and Gerber, R. B.: Nitrogen dioxide at the air-water interface: Trapping, absorption, and solvation in the bulk and at the surface, Phys. Chem. Chem. Phys., 15, 204–212, doi:10.1039/c2cp42810e, 2013.

Myneni, R. B., Hoffman, S., Knyazikhin, Y., Privette, J. L., Glassy, J., Tian, Y., Wang, Y., Song, X., Zhang, Y., Smith, G. R., Lotsch, A., Friedl, M., Morisette, J. T., Votava, P., Nemani, R. R. and Running, S. W.: Global products of vegetation leaf area and fraction absorbed PAR from year one of MODIS data, Remote Sens. Environ., 83(1–2), 214–231, doi:10.1016/S0034-4257(02)00074-3, 2002.

Neirynck, J. and Ceulemans, R.: Bidirectional ammonia exchange above a mixed coniferous forest, Environ. Pollut., 154(3), 424–438, doi:10.1016/j.envpol.2007.11.030, 2008.

Nemitz, E., Sutton, M. A., Schjoerring, J. K., Husted, S. and Paul Wyers, G.: Resistance modelling of ammonia exchange over oilseed rape, Agric. For. Meteorol., 105(4), 405–425, doi:10.1016/S0168-1923(00)00206-9, 2000.

Nguyen, T. B., Crounse, J. D., Teng, A. P., St. Clair, J. M., Paulot, F., Wolfe, G. M. and Wennberg, P. O.: Rapid deposition of oxidized biogenic compounds to a temperate forest, Proc. Natl. Acad. Sci., 112(5), E392–E401, doi:10.1073/pnas.1418702112, 2015.

Nobel, P. S.: Physicochemical and Environmental Plant Physiology, 4th ed., Elsevier., 2009.

Nobel, P. S., Zaragoza, L. J. and Smith, W. K.: Relation between Mesophyll Surface Area, Photosynthetic Rate, and Illumination Level during Development for Leaves of Plectranthus parviforus Henckel, Plant Physiol., 55, 1067–1070, doi:10.1104/pp.55.6.1067, 1975.

Novakov, T.: Laboratory Study of NO2 Reaction with Dispersed and Bulk Liquid Water--Author's Reply, Atmos. Environ., 29(18), 2559–2560, 1995.

Nowlan, C. R., Martin, R. V., Philip, S., Lamsal, L. N., Krotkov, N. A., Marais, E. A., Wang, S. and Zhang, Q.: Global dry deposition of nitrogen dioxide and sulfur dioxide inferred from space-based measurements, Global Biogeochem. Cycles, 28, doi:10.1002/2014GB004805, 2014.

Oke, T. R.: Boundary Layer Climates, 2nd ed., Routledge., 1987.

Panofsky, H. A.: Determination of stress from wind and temperature measurements, Q. J. R. Meteorol. Soc., 89(379), 85–94, doi:10.1002/qj.49708937906, 1963.

Pariyar, S., Eichert, T., Goldbach, H. E., Hunsche, M. and Burkhardt, J.: The exclusion of ambient aerosols changes the water relations of sunflower (Helianthus annuus) and bean (Vicia faba) plants, Environ. Exp. Bot., 88, 43–52, doi:10.1016/j.envexpbot.2011.12.031, 2013.

Physick, W. L. and Garratt, J. R.: Incorporation of a high-roughness lower boundary into a mesoscale model for studies of dry deposition over complex terrain, Boundary-Layer Meteorol., 74, 55–71, doi:10.1007/BF00715710, 1995.

Place, B. K., Delaria, E. R., Liu, A. X. and Cohen, R. C.: Leaf Stomatal Control over Acyl Peroxynitrate Dry Deposition to Trees, ACS Earth Sp. Chem., 4, 2162–2170, doi:10.1021/acsearthspacechem.0c00152, 2020.

Plake, D., Stella, P., Moravek, A., Mayer, J. C., Ammann, C., Held, A. and Trebs, I.: Comparison of ozone deposition measured with the dynamic chamber and the eddy covariance method, Agric. For. Meteorol., 206, 97–112, doi:10.1016/j.agrformet.2015.02.014, 2015.

Ramge, P., Badeck, F. -W., PLÖCHL, M. and KOHLMAIER, G. H.: Apoplastic antioxidants as decisive elimination factors within the uptake process of nitrogen dioxide into leaf tissues, New Phytol., 125, 771–785, doi:10.1111/j.1469-8137.1993.tb03927.x, 1993.

Raupach, M. R., Finnigan, J. J. and Brunet, Y.: Coherent eddies and turbulence in vegetation canopies: the mixing-layer analogy, Boundary-Layer Meteorol., 78(3–4), 351–382, doi:10.1007/BF00120941, 1996.

Ren, Y., Stieger, B., Spindler, G., Grosselin, B., Mellouki, A., Tuch, T., Wiedensohler, A. and Herrmann, H.: Role of the dew water on the ground surface in HONO distribution: a case measurement in Melpitz, Atmos. Chem. Phys., 20(2), 13069–13089, doi:10.5194/acp-20-13069-2020, 2020.

de Ridder, K.: Bulk transfer relations for the roughness sublayer, Boundary-Layer Meteorol., 134, 257–267, doi:10.1007/s10546-009-9450-y, 2010.

Rondón, A., Johansson, C. and Granat, L.: Dry deposition of nitrogen dioxide and ozone to coniferous forests, J. Geophys. Res., 98, 5159–5172, doi:10.1029/92JD02335, 1993.

Rovelli, G., Jacobs, M. I., Willis, M. D., Rapf, R. J., Prophet, A. M. and Wilson, K. R.: A critical analysis of electrospray techniques for the determination of accelerated rates and mechanisms of chemical reactions in droplets, Chem. Sci., 11(48), 13026–13043, doi:10.1039/d0sc04611f, 2020.

Schwartz, S. E. and Lee, Y. N.: Laboratory Study of NO2 Reaction with Dispersed and Bulk Liquid Water--Discussion, Atmos. Environ., 29(8), 2557–2559, 1995.

Sellers, P. J., Mintz, Y. and Dalcher, A.: A Simple Biosphere Model (SiB) for Use within General Circulation Models, J. Atmos. Sci., 43, 505–531, doi:10.1175/1520-0469(1986)043<0505:ASBMFU>2.0.CO;2, 1986.

Shah, V., Jaeglé, L., Thornton, J. A., Lopez-Hilfiker, F. D., Lee, B. H., Schroder, J. C., Campuzano-Jost, P., Jimenez, J. L., Guo, H., Sullivan, A. P., Weber, R. J., Green, J. R., Fiddler, M. N., Bililign, S., Campos, T. L., Stell, M., Weinheimer, A. J., Montzka, D. D. and Brown, S. S.: Chemical feedbacks weaken the wintertime response of particulate sulfate and nitrate to emissions reductions over the eastern United States, Proc. Natl. Acad. Sci. U. S. A., 115(32), 8110–8115, doi:10.1073/pnas.1803295115, 2018.

Silva, S. J. and Heald, C. L.: Investigating dry deposition of ozone to vegetation, J. Geophys. Res. Atmos., 123, 559–573, doi:10.1002/2017JD027278, 2018.

Simpson, I. J., Thurtell, G. W., Neumann, H. H., Den Hartog, G. and Edwards, G. C.: The validity of similarity theory in the roughness sublayer above forests, Boundary-Layer Meteorol., 87(1), 69–99, doi:10.1023/A:1000809902980, 1998.

Spataro, F. and Ianniello, A.: Sources of atmospheric nitrous acid: State of the science, current research needs, and future prospects, J. Air Waste Manage. Assoc., 64(11), 1232–1250, doi:10.1080/10962247.2014.952846, 2014.

Stella, P., Kortner, M., Ammann, C., Foken, T., Meixner, F. X. and Trebs, I.: Measurements of nitrogen oxides and ozone fluxes by eddy covariance at a meadow: Evidence for an internal leaf resistance to NO2, Biogeosciences, 10(9), 5997–6017, doi:10.5194/bg-10-5997-2013, 2013.

Stocker, D. W., Zeller, K. F. and Stedman, D. H.: O3 and NO2 fluxes over snow measured by eddy correlation, Atmos. Environ., 29(11), 1299–1305, doi:10.1016/1352-2310(94)00337-K, 1995.

Stroud, C., Makar, P., Karl, T., Guenther, A., Geron, C., Turnipseed, A., Nemitz, E., Baker, B., Potosnak, M. and Fuentes, J. D.: Role of canopy-scale photochemistry in modifying biogenic-atmosphere exchange of reactive terpene species: Results from the CELTIC field study, J. Geophys. Res., 110, D17303, doi:10.1029/2005JD005775, 2005.

Su, H., Cheng, Y., Oswald, R., TBehrendt, T., Trebs, I., Meixner, F. X., Andreae, M. O., Cheng, P., Zhang, Y. and Poschl, U.: Soil Nitrite as a Source of Atmospheric HONO and OH Radicals, Science (80-.)., 333(6049), 1616–1618, doi:10.1126/science.1207687, 2011.

Sun, S., Moravek, A., Trebs, I., Kesselmeier, J. and Sörgel, M.: Investigation of the influence of liquid surface films on O3 and PAN deposition to plant leaves coated with organic/inorganic solution, J. Geophys. Res. Atmos., 121, 14,239-14,256, doi:10.1002/2016JD025519, 2016.

Tang, M. J., Cox, R. A. and Kalberer, M.: Compilation and evaluation of gas phase diffusion coefficients of reactive trace gases in the atmosphere: Volume 1. Inorganic compounds, Atmos. Chem. Phys., 14(17), 9233–9247, doi:10.5194/acp-14-9233-2014, 2014.

Tang, M. J., Shiraiwa, M., Pöschl, U., Cox, R. A. and Kalberer, M.: Compilation and evaluation of gas phase diffusion coefficients of reactive trace gases in the atmosphere: Volume 2. Diffusivities of organic compounds, pressure-normalised mean free paths, and average Knudsen numbers for gas uptake calculations, Atmos. Chem. Phys., 15(10), 5585–5598, doi:10.5194/acp-15-5585-2015, 2015.

Teklemariam, T. A. and Sparks, J. P.: Leaf fluxes of NO and NO2 in four herbaceous plant species: The role of ascorbic acid, Atmos. Environ., 40(12), 2235–2244, doi:10.1016/j.atmosenv.2005.12.010, 2006.

Thoene, B., Rennenberg, H. and Weber, P.: Absorption of atmospheric NO2 by spruce (Picea abies) trees: II. Parameterization of NO2 fluxes by controlled dynamic chamber experiments, New Phytol., 134(2), 257–266, doi:10.1111/j.1469-8137.1996.tb04630.x, 1996.

Toyota, K., Dastoor, A. P. and Ryzhkov, A.: Parameterization of gaseous dry deposition in atmospheric chemistry models: sensitivity to aerodynamic resistance formulations under statically stable conditions, Atmos. Environ., 147, 409–422, doi:10.1016/j.atmosenv.2016.09.055, 2016.

Trumbore, S. E., Keller, M., Wofsy, S. C. and DA Costa, J. M.: Measurements of soil and canopy exchange rates in the amazon rain forest using 222Rn, J. Geophys. Res., 95(D10), 16865–16873, doi:10.1029/JD095iD10p16865, 1990.

Turnipseed, A. A., Huey, L. G., Nemitz, E., Stickel, R., Higgs, J., Tanner, D. J., Slusher, D. L., Sparks, J. P., Flocke, F. and Guenther, A.: Eddy covariance fluxes of peroxyacetyl nitrates (PANs) and NOy to a coniferous forest, J. Geophys. Res., 111, D09304, doi:10.1029/2005JD006631, 2006.

Walton, S., Gallagher, M. W., Choularton, T. W. and Duyzert, J.: Ozone and NO2 exchange to fruit orchards, Atmos. Environ., 31(17), 2767–2776, doi:10.1016/S1352-2310(97)00096-4, 1997.

Wang, W., Ganzeveld, L., Rossabi, S., Hueber, J. and Helmig, D.: Measurement report: Leaf-scale gas exchange of atmospheric reactive trace species (NO2, NO, O3) at a northern hardwood forest in Michigan, Atmos. Chem. Phys., 20(19), 11287–11304, doi:10.5194/acp-20-11287-2020, 2020.

Wang, Y., Jacob, D. J. and Logan, J. A.: Global simulation of tropospheric O3-NOx-hydrocarbon chemistry: 1. Model Formulation, J. Geophys. Res., 103(D9), 10713–10725, doi:10.1029/98JD00158, 1998.

Wen, D., Zhang, L., Lin, J. C., Vet, R. and Moran, M. D.: An evaluation of ambient ammonia concentrations over southern Ontario simulated with different dry deposition schemes within STILT-Chem v0.8, Geosci. Model Dev., 7(3), 1037–1050, doi:10.5194/gmd-7-1037-2014, 2014.

Wentworth, G. R., Murphy, J. G., Gregoire, P. K., Cheyne, C. A. L., Tevlin, A. G. and Hems, R.: Soil-atmosphere exchange of ammonia in a non-fertilized grassland: Measured emission potentials and inferred fluxes, Biogeosciences, 11(20), 5675–5686, doi:10.5194/bg-11-5675-2014, 2014.

Wenzel, A., Kalthoff, N. and Horlacher, V.: On the profiles of wind velocity in the roughness sublayer above a coniferous forest, Boundary-Layer Meteorol., 84(2), 219–230, doi:10.1023/A:1000444911103, 1997.

Wesely, M. L.: Parametrization of surface resistances to gaseous dry deposition in regional-scale numerical models, Atmos. Environ., 23(6), 1293–1304, doi:10.1016/0004-6981(89)90153-4, 1989.

Wesely, M. L. and Hicks, B. B.: Some factors that affect the deposition rates of sulfur dioxide and similar gases on vegetation, J. Air Pollut. Control Assoc., 27(11), 1110–1116, doi:10.1080/00022470.1977.10470534, 1977.

Wolfe, D. E. and Lataitis, R. J.: Boulder Atmospheric Observatory: 1977–2016: The end of an era and lessons learned, Bull. Am. Meteorol. Soc., 99(7), 1345–1358, doi:10.1175/BAMS-D-17-0054.1, 2018.

Wong, A. Y. H., Geddes, J. A., Tai, A. P. K. and Silva, S. J.: Importance of dry deposition parameterization choice in global simulations of surface ozone, Atmos. Chem. Phys., 19, 14365–14385, doi:10.5194/acp-19-14365-2019, 2019.

Yabushita, A., Enami, S., Sakamoto, Y., Kawasaki, M., Hoffmann, M. R. and Colussi, A. J.: Anion-catalyzed dissolution of NO2 on aqueous microdroplets, J. Phys. Chem. A, 113(17), 4844–4848, doi:10.1021/jp900685f, 2009.

Yienger, J. J. and Levy II, H.: Empirical model of global soil-biogenic NOx emissions, J. Geophys. Res., 100(D6), 11447–11464, doi:10.1029/95JD00370, 1995.

Zhang, L., Brook, J. R. and Vet, R.: A revised parameterization for gaseous dry deposition in air-quality models, Atmos. Chem. Phys., 3, 2067–2082, doi:10.5194/acp-3-2067-2003, 2003.